Escherichia coli K1 utilises host macropinocytic pathways for invasion of brain microvascular endothelial cells

Lip Nam Loh[1†], Elizabeth M. C. McCarthy[1], Priyanka Narang[1‡], Naveed A. Khan[2], and Theresa H. Ward[1*]

Affiliations:

[1] Department of Immunology and Infection, Faculty of Infectious and Tropical Diseases, London School of Hygiene and Tropical Medicine, London, UK.

[2] Department of Biological Sciences, Faculty of Science and Technology, Sunway University, 47500 Selangor, Malaysia.

*Corresponding author: Tel. (+44) 207 927 2649; Fax (+44) 207 323 5687; email theresa.ward@lshtm.ac.uk

[†]Present address: Departments of Pediatrics, and Microbiology and Immunology, Albert Einstein College of Medicine, Bronx, NY, USA

[‡]Present address: Envision Pharma Group, Horsham, UK

Key words:
Escherichia coli, neonatal meningitis, dynamin, clathrin-independent endocytosis, Rho GTPase family, macropinocytosis

Running title:
E. coli K1 invades HBMEC via macropinocytosis

Synopsis
Several clathrin-independent endocytic pathway components have been implicated as regulatory factors exploited by neonatal meningitis-causing *Escherichia coli* K1 bacteria to infect host cells. Here we demonstrate that the bacteria induce general cell ruffling, increased fluid phase uptake, and actin-, Rho GTPase- and cholesterol-dependent invasion, which all point to a requirement for macropinocytosis as the route of uptake by the bacteria into non-phagocytic brain microvascular endothelial cells.

Abstract

Eukaryotic cells utilise multiple endocytic pathways for specific uptake of ligands or molecules, and these pathways are commonly hijacked by pathogens to enable host cell invasion. *Escherichia coli* K1, a pathogenic bacterium that causes neonatal meningitis, invades the endothelium of the blood-brain barrier, but the entry route remains unclear. Here we demonstrate that the bacteria trigger an actin-mediated uptake route, stimulating fluid phase uptake, membrane ruffling and macropinocytosis. The route of uptake requires intact lipid rafts as shown by cholesterol depletion. Using a variety of perturbants we demonstrate that small Rho GTPases and their downstream effectors have a significant effect on bacterial invasion. Furthermore, clathrin-mediated endocytosis appears to play an indirect role in *E. coli* K1 uptake. The data suggest that the bacteria effect a complex interplay between the Rho GTPases to increase their chances of uptake by macropinocytosis into HBMEC.

Introduction

Neonatal bacterial meningitis (NBM) is a life-threatening disease that progresses rapidly, and, despite advances in chemotherapy and supportive care that have reduced overall case numbers, at least in industrialised countries, up to 50% of survivors are left with long-term disability and serious neurological dysfunction (1-4). The *Escherichia coli* strain carrying the K1 capsule is globally the most common cause of NBM in early neonates (only surpassed by Group B streptococcus in the developed world), and mortality rates remain high at 10-58% (1,3-8).

Several bacterial virulence factors are thought to contribute to bacterial traversal of the blood-brain barrier (BBB), a critical step to penetrate the brain and cause the disease pathophysiology (9). Bacterial adherence to receptors on the surface of human brain microvascular endothelial cells (HBMEC) stimulates the activation of host molecules involved in a number of signalling pathways, including signal transducer and activator of transcription 3 (stat3), focal adhesion kinase (FAK), phosphatidylinositol-3-kinase (PI3K), protein kinase Cα (PKCα), p21-associated kinase 1 (PAK1) and the small GTPases Rac1 and RhoA (10-17). These signalling events result in actin polymerisation at the bacterial adhesion site, which is necessary for bacterial internalisation into HBMEC (18). However, the specific endocytic pathway hijacked by the bacterial invasion of HBMEC is not well characterised (19,20), and could contribute to identification of targets for prevention and therapy of *E. coli* meningitis.

Here, using perturbation of endocytosis by overexpression of functional mutant proteins and by inhibition with small compound inhibitors and siRNA (20), in conjunction with fluorescence microscopy and quantitative flow cytometry-based assays, we demonstrate that the bacteria exploit fluid-phase uptake, or macropinocytic, pathways to gain entry into HBMEC cells. We show that this invasion

process is actin-mediated, that it coordinates the collective activity of the small GTPases of the Rho family (RhoA, Rac1 and Cdc42) and downstream effectors (including PAK1, PKC and PI3K), and requires cholesterol to enable phagocytic-like uptake of *E. coli* K1 into the host cells.

Results

E. coli K1 invasion of HBMEC is dependent upon actin recruitment

The current literature has identified host-specific signalling molecules that contribute to *E. coli* K1 interaction with HBMEC cells but remains unclear on the uptake pathway that leads to cell invasion (12,15,17,21,22). Therefore we have taken a first principles approach to investigate the route of endocytic invasion of HBMEC by *E. coli* K1.

Actin polymerisation plays a role in multiple endocytic pathways (19,20). To study the relation of actin to invading bacteria, HBMEC were infected with *E. coli* K1 bacteria for 30 min, then fixed and stained for extracellular and intracellular bacteria sequentially in conjunction with phalloidin staining to label actin. Bacteria at the cell surface showed association with ruffling membrane denoted by actin filaments (Fig. 1A, B). Invading bacteria were surrounded by an actin cup (Fig. 1B). Internalised bacteria were found with and without actin coats (Fig. 1C and 1D, respectively). Quantitation of bacteria with and without actin at different timepoints following infection (Supp. Fig. 1C) suggests a role for actin in coating the bacterial vacuole during its formation and the actin then depolymerises once the bacterium is fully internalised. The role of the cytoskeleton in bacterial uptake was therefore further investigated using cytoskeleton perturbation agents. Cells were pretreated with several inhibitors (Fig. 1E) and then infected with *E. coli* K1 for 1 hr. The F-actin depolymerising agent cytochalasin D, the F-actin stabilising agent jasplakinolide, or blebbistatin, an inhibitor of myosin II which has been shown to drive closure of actin cups, all significantly inhibited bacterial invasion while nocodazole, a microtubule-destabilising agent, had no effect (Fig. 1E). These results demonstrated that, while microtubules were not required, actin played an important role in bacterial entry and infection.

Through timelapse imaging of HBMEC expressing an actin reporter, the host cells were found to respond directly to *E. coli* K1. Actin-based membrane ruffling throughout the cell surface was induced from 5-10 min following exposure to the bacteria, with the cells becoming quiescent from 25-30 min (Supp. Movie 1; Supp. Fig. 1A, B). Following this time series, a z-stack of one cell shows an internalised bacterium (Supp. Fig. 1B). Quantitation of actin showed that ruffling was induced by *E. coli* K1 but not by non-pathogenic *E. coli* K-12 (Supp. Fig. 1D). This suggests that the bacteria induce actin mobilisation to upregulate the cell's uptake pathways to enable cell entry.

Involvement of actin-modulating small GTPases in *E. coli* K1 invasion

Previous publications have implicated the actin recruitment proteins RhoA and Rac1 with putative roles in *E. coli* K1 invasion (12,15,17). The Rho GTPases cycle between a GTP-bound, active, state and a GDP-bound, inactive, state. Activity can be modulated by expression of dominant mutants which alter nucleotide binding. To study involvement of the Rho family of GTPases during bacterial invasion quantitatively, HBMEC were transiently transfected with GFP chimaeric constructs of the GTPases and their related mutants. A plasmid encoding GFP alone was transfected into HBMEC as a transfection control. Transfected cells were infected with *E. coli* K1 bacteria expressing mCherry (K1-Cherry) for 2 hr, incubated for 1 hr in media containing gentamicin to kill extracellular bacteria, processed for imaging, and then tiled z-stack confocal images were acquired to obtain a large unbiased field. Quantification of GFP-positive cells with intracellular K1-Cherry showed that cells transfected with activated RhoA (RhoA V14) and Rac1 (Rac1 L61) both had significantly higher number of cells with internalised bacteria, while cdc42 activated mutant (cdc42 V12) had no significant effect on bacterial uptake when compared to wild type but did significantly increase number of cells with bacterial uptake when compared to the inactive mutant, cdc42 N17 and the GFP control (Fig. 2A). Furthermore, the inactive mutants of RhoA and Rac1 showed significant reduction in number of infected cells relative to the GFP control. In the case of all GTPase constructs some internalised bacteria could be seen to colocalise with a concentrated ring of GFP stain while others were found without any specific colocalisation (Fig. 2B,C shows cdc42 as an example of this). As bacterial uptake was not tightly synchronised, this would suggest that during invasion the bacteria transiently associate with membranes to which the small GTPases are recruited and these are then released from the membrane as the bacterial vacuole matures.

The effect of inhibition of downstream effectors of the Rho GTPases including p21-activated kinase 1 (PAK1), protein kinase C (PKC) and phosphatidylinositol-3-kinase (PI3K) with IPA-3, GF109203X and wortmannin, respectively, was next tested. These inhibitors were found to significantly block entry of bacteria into cells (Fig. 2D). In comparison, transferrin uptake, used as a marker for clathrin-mediated endocytosis (CME), was not inhibited by any of the kinase inhibitors tested, indeed PKC inhibition led to increased transferrin uptake. Furthermore, uptake of labelled dextran, a marker for fluid phase uptake, was found to be markedly inhibited only by wortmannin treatment (Fig. 2D). To further investigate activation of signalling pathways, total cell lysates were analysed by Western blot with antibodies to phosphorylated Akt, a downstream effector of PI3K (Fig. 7C,D). As found in previous studies, Akt was transiently phosphorylated following infection of HBMEC (16).

Together these results support a role for Rho GTPases, and their downstream effectors, in *E. coli* K1 invasion of HBMEC.

***E. coli* K1 invasion of HBMEC is cholesterol-dependent**

The involvement of actin, the membrane ruffling and the importance of nonspecific Rho GTPase activity and the regulatory kinases all point to macropinocytosis or another clathrin-independent pathway as a potential entry mechanism for *E. coli* K1 into the endothelial cells (23). As cholesterol is required for membrane ruffling, lipid raft dependent endocytosis (such as caveolae) and macropinocytosis (24-26), the effect of HBMEC treatment with methyl-β-cyclodextrin (MβCD), a reagent used to deplete membrane cholesterol, was tested on the uptake of *E. coli* K1. Bacterial invasion was significantly inhibited by >95% upon cholesterol depletion (Fig. 3A). Conversely, cholesterol loading of HBMEC cells through the addition of water-soluble cholesterol (MβCD-cholesterol complexes) increased bacterial invasion by 79%±16% (Fig. 3A). These data indicated the importance of cholesterol and associated lipid rafts in *E. coli* K1 invasion of HBMEC.

As a comparison, the effect of cholesterol depletion with MβCD and cholesterol loading on the endocytic markers transferrin (for clathrin-mediated uptake) and dextran (for fluid phase uptake) was also explored (Fig. 3B). Cholesterol depletion had an inhibitory effect on dextran uptake while transferrin uptake was enhanced by cholesterol depletion, both with dose-dependent effect. Therefore *E. coli* K1 uptake again more closely resembled the dynamics of the fluid phase pathway in response to cholesterol depletion treatment.

***E. coli* K1 invasion of HBMEC is caveolin-1-independent**

Caveolae-mediated endocytosis is highly sensitive to cholesterol-depleting agents (27), and has previously been implicated in *E. coli* K1 invasion of HBMEC (21,22). To investigate this possible uptake route, HBMEC were infected with *E. coli* K1-Cherry, fixed at indicated time points post infection, and immunolabelled for caveolin-1. After 30 min of infection, some bacteria could be found localised in compartments weakly labelled for caveolin-1 (Fig. 4A, white arrows). However, quantification showed that only about 4% of the bacteria were closely associated with caveolin-1 after 30 min infection (Fig. 4B), which was further reduced to about 1% at 2 hr post infection (p.i.) and continued to diminish at later timepoints. Therefore, association of *E. coli* K1 with caveolin-1 seemed to be a rare event, occurring at early time points of infection, presumably during internalisation.

While these data suggested that caveolae-mediated uptake was not a major route of invasion for *E. coli* K1 into HBMEC, it was possible that the interaction with caveolin may be too fleeting to record. However, expression of a dominant caveolin-1 mutant that inactivates caveolae-dependent uptake (caveolin-1-Tyr14; 28,29) had no effect on *E. coli* K1 invasion into HBMEC (Fig. 4C). Furthermore, bacterial invasion of either caveolin-1 knockout (Cav1 KO) endothelial cells compared to wild type cells (WT), or caveolin-1 knockdown in HBMEC with siRNA, in both cases revealed that loss of caveolin-1 resulted in a significant increase in *E. coli* K1 invasion (Fig. 4D and 4E, respectively), indicating that the presence of caveolin-1 was not essential for bacterial entry. As caveolin-2 expression is suppressed by knockdown of caveolin-1, it is not possible that this is acting in a compensatory manner (30-33).

Overall, our data therefore indicated that *E. coli* K1 invasion of HBMEC is not dependent on caveolae-mediated endocytosis.

***E. coli* K1 invasion of HBMEC is dynamin-dependent**

Many endocytic routes, including clathrin-mediated, caveolae and some lipid-raft-dependent uptake routes, require recruitment of dynamin (Dyn), a large GTPase necessary for pinching off transport intermediates from the plasma membrane. Overexpression of the GDP-locked dynamin mutant inhibits these uptake routes (34-36). We therefore hypothesised that, if the bacteria invaded HBMEC in a dynamin-dependent manner, overexpression of Dyn2(aa)K44A (37), would inhibit *E. coli* K1 invasion of HBMEC. HBMEC were transiently transfected with GFP-tagged Dyn2 chimaeric constructs, with a plasmid encoding GFP alone used as a transfection control. Following infection with K1-Cherry for 30 min, bacteria at the cell surface showed no specific colocalisation with dynamin, nor were any intracellular bacteria encircled by dynamin stain (Supp. Fig. 2C) as has been seen previously with invading bacteria such as *Listeria monocytogenes* (38). Quantification of GFP-positive cells with intracellular K1-Cherry showed no inhibition of bacterial invasion in cells overexpressing Dyn2(aa)K44A GFP (Fig. 5A), contrary to what would be expected for a dynamin-dependent uptake route. Repetition of the experiments with Dyn1 constructs confirmed these results, and no reduction in *E. coli* K1 invasion of HBMEC overexpressing dominant negative Dyn1 (Dyn1K44A-GFP) was seen (Fig. 5A). In fact, there was a modest enhancement in *E. coli* K1 internalisation into these cells compared to cells expressing wild type Dyn1, although it was not statistically significant.

To demonstrate that the dynamin mutant had a significant effect on the dynamin-dependent uptake pathways in these cells, a control transferrin uptake experiment was performed with either Dyn2(aa)WT-GFP or Dyn2(aa)K44A-GFP expressing cells. Supp. Fig. 2A and 2B demonstrate that transferrin uptake is abrogated in cells expressing GFP-tagged mutant Dyn2. Furthermore, when the chimaeric Dyn2 constructs were expressed in HBMEC and the cells were infected with *L. monocytogenes*, uptake was inhibited by both the dominant mutant and by overexpression of the wild type Dyn2 construct itself (Fig. 5B).

We further tested the role of dynamin by using the inhibitory agent dynasore to inhibit dynamin in the *E. coli* K1 invasion assay. Only at high concentration was dynasore found to inhibit *E. coli* K1 uptake (Fig. 5C). In contrast, dynasore had a significant impact on *Listeria* invasion at the lowest concentration tested (Fig. 5C). At high concentrations dynasore inhibits fluid-phase endocytosis in a dynamin-independent manner (Supp. Fig. 3A; 39), which may explain why *E. coli*

K1 invasion is only affected at high concentration. The effect of Dyn2 depletion through siRNA transfection on *E. coli* K1 uptake was investigated. Relatively inefficient knockdown was achieved in the HBMEC cells, however, with a 45% reduction in Dyn2 levels, a 40% reduction in bacterial invasion was seen (Fig. 5D).
This suggests that, while dynamin had some effect on *E. coli* K1 invasion, it was not as clear a role as seen with *L. monocytogenes* infection.

E. coli K1 upregulates macropinocytosis and utilises the pathway to invade HBMEC

To further explore the role of macropinocytosis in *E. coli* K1 invasion, the effect of bacteria on fluid phase uptake was investigated. Internalisation of fluid by macropinocytosis can be stimulated with high levels of serum (40,41). FITC-dextran, employed as a marker for fluid phase uptake during macropinocytosis, was added to serum-starved HBMEC in low or high serum medium, or in conjunction with bacterial infection, and cells were then analysed by flow cytometry for FITC content (Fig. 6A). The experimental medium used for bacterial invasion had a low serum content, and the high serum experimental medium was employed as a positive control for macropinocytic uptake in HBMEC (40,41). Analysis of FITC levels revealed that high serum induced a small but reproducible and significant shift in median FITC measurements, indicative of increased fluid phase uptake in cells stimulated with serum (Fig. 6A). FITC-dextran internalisation was also increased relative to low-serum media alone upon exposure to *E. coli* K1 (Fig. 6A), indicating that bacteria increase fluid-phase uptake in HBMEC.
Activity of the Na^+/H^+ exchanger at the plasma membrane modulates Rho GTPases and this can be inhibited by the amiloride-derivative 5-(N-Ethyl-N-isopropyl) amiloride (EIPA) thereby inhibiting macropinosome formation (42). Another reagent often used as a macropinocytosis inhibitor is rottlerin, potentially acting through PKC although its mechanism of action is unclear (23,43). Treatment of HBMEC with either EIPA or rottlerin had a strong inhibitory effect on fluid-phase uptake as measured by labelled 10 kDa dextran internalisation (Fig. 6B). Clathrin-mediated uptake of transferrin was not inhibited by these treatments, and rottlerin induced a strong increase in transferrin uptake compared to the control. EIPA and rottlerin reduced *E. coli* K1 invasion by 95% and 99%, respectively (Fig. 6B), indicating that *E. coli* K1 requires macropinocytosis in order to infect HBMEC cells. When cells were infected with *E. coli* K1 in the presence of Alexa Fluor 647-dextran for 30 min, fixed and stained for extra- and intracellular bacteria and then imaged, labelled dextran colocalised with internalised bacteria (Fig. 6C). Quantification of internalised bacteria associated with dextran following 30 min uptake showed that 59.7±4.9% bacteria were in dextran-positive compartments (Fig. 6D). These data indicated that the bacteria entered through the macropinocytic pathway.

Clathrin-mediated endocytosis is indirectly involved in _E. coli_ K1 invasion

Although clathrin has not been found associated with bacterial vacuoles as visualised by microscopy (18), the involvement of clathrin-mediated uptake in *E. coli* K1 invasion has not been quantitatively measured. Chlorpromazine (CPZ) is a pharmacologic inhibitor of clathrin-mediated endocytosis but has off-target effects that can vary between cell types (44-46). When the effect of CPZ on bacterial invasion of HBMEC was assessed, no significant inhibition of *E. coli* K1 invasion was found across a range of concentrations (Fig. 7A). Although there appeared to be decreased efficiency in invasion with lower concentrations of CPZ, this was not statistically significant. In contrast, invasion of *L. monocytogenes*, which enters cells utilising the CME pathway components (38,47), was inhibited by CPZ in dose-dependent manner (Fig. 7A). When the effect of CPZ on endocytic markers was tested, transferrin uptake showed a small but significant inhibitory effect, while dextran was unaffected (Supp. Fig. 3A). In support of the earlier study by Prasadarao *et al* (18), we also found no association of clathrin with bacterial vacuoles containing *E. coli K1*, while *Listeria* bacteria were found to colocalise with clathrin (Supp. Fig. 3B). This supports *E. coli* K1 invasion through a non-clathrin-mediated pathway.
Specific targeting of clathrin-mediated uptake through siRNA depletion of adaptor protein complex 2 (AP2) resulted in a decrease of 80% in *E. coli* K1 invasion (Fig. 7B). This somewhat contradicted the CPZ result and suggested that clathrin might be the major uptake pathway for *E. coli* K1. However, when cells were also treated with EIPA, to additionally block macropinocytosis, bacterial invasion was 95% inhibited (Fig. 7B).
When the effect of AP2 depletion on *E. coli*-stimulated Akt phosphorylation was examined through immunoblotting of cell lysates (Fig. 7C,D), this revealed that Akt phosphorylation was greatly reduced compared to control (approximately 50% level of phospho-Akt) at 30 min post infection.
This would suggest that a long-term block in clathrin-mediated uptake, as in an siRNA transfection timecourse, reduced an important plasma membrane component for *E. coli* K1 invasion, diminishing both invasion and signalling. Since trafficking through clathrin-independent endocytic routes has been found to exhibit some dependency on clathrin-mediated endocytosis (48), this may explain the apparent effect of CME blocks on *E. coli* K1 invasion.

Discussion

In order to establish meningitis, *E. coli* K1 must induce its uptake by the endothelial cells that form the blood-brain barrier, and then traverse these cells. These microvascular endothelial cells are known to have very few endocytic vesicles (49), which may derive from any of the clathrin-dependent or -independent endocytic pathways (19). Therefore, in order to gain entry to the cells, the bacteria must induce huge changes in uptake dynamics. The actin-mediated membrane ruffling seen here at the cell surface points to bacteria-induced upregulation of macropinocytic activity. This enables a phagocytic-like uptake of the bacteria.

The requirement for actin in *E. coli* K1 uptake into HBMEC has been demonstrated by both accumulation of host actin to the membrane underlying invading bacteria, by the increased actin mobilisation seen in the live imaging, and by the inhibitory effects on bacterial invasion by actin inhibitors (here and (18)). The small GTPases of the Rho family (Rho, Rac1 and cdc42) are frequently involved in the signalling cascade which regulates actin filament dynamics leading to membrane ruffling (23). The bacterial toxin cytotoxic necrotizing factor 1 (CNF1), produced by pathogenic *E. coli* bacteria including *E. coli* K1, coordinately activates Rho, Rac and Cdc42 (12,50,51), which in turn upregulate generalised ruffling activity and actin recruitment, the processes which underlie induction of macropinocytosis. Previous investigations have suggested that both RhoA (through CNF1) and Rac1 (through outer membrane protein A, OmpA) play a role in *E. coli* K1 uptake (12,15,17). Here we have demonstrated that activated RhoA, Rac1 and cdc42 can promote *E. coli* K1 invasion, and that this may be linked to PAK1 and PI3K activation. Signalling through the PI3K pathway culminates in phosphorylation of Akt, which has been found to also require PAK1 and PKCα for efficient activation (52,53). CNF1 from *E. coli* K1 may therefore act in concert with OmpA to switch on the collective activity of the GTPases and their downstream effectors to bring about cytoskeletal rearrangement to form macropinosomes (Fig. 8) (12,17,18). Cdc42 and Rac1 both constitute major regulators of macropinocytosis (20,23,54), but while RhoA has not been considered a factor in macropinocytosis, it has been implicated in lipid raft-mediated endocytic pathways (19,20). Furthermore, the precedent for additional Rho GTPase family members to be required for macropinocytosis in concert with Rac1 and Cdc42 has been shown with *Salmonella* invasion of non-phagocytic cells (55), where RhoG was required, together with Rac1 and Cdc42, to orchestrate actin modulation required for bacterial entry. The ability to manipulate bacterial invasion by all the Rho GTPases suggests that the bacterial invasion requires a dynamic activation of actin recruitment to upregulate macropinocytosis in order for the bacteria to force cell engulfment.

Virus induction of macropinocytosis is often associated with activation of signalling pathways that lead to changes in actin dynamics, causing membrane ruffling and increased fluid phase uptake, which results in internalisation of particles including viruses as well as fluid (54,56). Plasma membrane deformation during macropinocytosis differs from phagocytosis in that the latter specifically forms a membrane cup around an object targeted by the cell for uptake, while the former involves indiscriminate cell-wide membrane ruffling. Different macropinocytic mechanisms show distinct membrane formations and, while some macropinocytic events rely on induction of circular ruffling, others are characterised by plasma membrane deformation as either flat lamellipodial sheets or as blebs (57,58). In our data, bacterial addition resulted in non-specific membrane ruffling with no evident circular formations. We also saw increased fluid uptake upon exposure of the endothelial cells to *E. coli* K1 which concurs with the electron micrographs of internalised bacteria in the previous study by Prasadarao *et al* that showed internalised bacteria surrounded by notable amounts of fluid in their vacuoles (18). Together, the transient membrane ruffling response of the cells to the bacteria, involvement of multiple Rho GTPases, stimulated dextran uptake and inhibition by macropinocytic inhibitory reagents all point to indiscriminate stimulation of particle uptake mechanisms to enable bacterial invasion by macropinocytic-like processes. This is also termed triggered phagocytosis (56).

Methyl-β-cyclodextrin has been shown before to inhibit *E. coli* K1 entry into HBMEC (22). The mechanism of this inhibition is unknown and could be due to effects on cell surface receptor expression such as by receptor sequestration or by inhibition of receptor-mediated invasion. However, new data shown here demonstrates that cholesterol loading of the cells has the opposite effect, where the bacteria can much more readily gain entry to the cells. This cannot be easily explained by a large increase in receptors on the surface and suggests that the levels of cholesterol in the cell membrane may alter the environment in another way to facilitate bacterial invasion. Depletion of cholesterol from membranes might remove some important receptor from the cell membranes, hence preventing uptake, however cholesterol loading would not be expected to cause upregulation of an equivalent receptor during the short treatment time to explain the increased uptake and therefore this points to a more direct effect of cholesterol itself.

While previous studies of *E. coli* K1 invasion have implicated a role for caveolae for bacterial entry into HBMEC (21,22), we could find no evidence for a role for caveolae through both direct visualised association of a caveolin coat, through inhibitory effects of dominant mutants, siRNA knockdown, and through use of a knockout cell line. We instead found increased bacterial invasion in cells with reduced caveolin-1. Since cholesterol is found concentrated in caveolae, they may have a role in regulating levels of cholesterol and other lipids in the plasma membrane (59,60). In caveolin null cells, there is no difference in total plasma membrane cholesterol compared to wild type cells (61,62), suggesting that the cholesterol usually sequestered within caveolae is distributed instead throughout the plasma membrane. This might lead to a membrane environment equivalent to our cholesterol loading experiment, that also led to increased invasion of HBMEC by *E. coli* K1. In agreement with this, in cells depleted of caveolin-1 fluid phase uptake is upregulated (63). Similarly, increased membrane microdomain mobility in caveolin null cells is attributed to enhanced invasion of *Staphylococcus aureus* (64).

Previously, clathrin has not been implicated in *E. coli* K1 uptake. Here we found an apparent effect with inhibition of clathrin-mediated endocytosis through both pharmacological inhibitors (of clathrin and dynamin) and through siRNA knockdown of AP2, the clathrin adaptor complex, although an earlier study, and our own data, could find no colocalisation with clathrin (18). Although the

chemical inhibitors used in this study are known to have off-target effects (44-46), the effects seen on *Listeria* uptake much more closely followed transferrin uptake as would be expected given its association with clathrin on entry, shown here and (38,47). However, in each case, *E. coli* K1 invasion dynamics showed very different behaviour. Dynasore inhibited *E. coli* K1 entry only at high concentrations. This reagent has been previously found to affect macropinocytosis, attributed to its inhibition of membrane ruffling and fluid phase uptake, which is dynamin-independent (39,65). Therefore this would explain its impact on uptake by *E. coli* K1 via a macropinocytic invasion route. Dynamin itself does not have a direct effect on macropinocytosis (39,40). That AP2 and dynamin knockdown have such a strong effect on *E. coli* K1 invasion may be due to an indirect effect such as preventing cell surface recycling of important plasma membrane protein components through CME (48). Alternatively, long term depletion of CME components could have an effect on cholesterol homeostasis by preventing internalisation of LDL at the plasma membrane (Fig. 8; 65).

Blood bacteraemia must reach a threshold before the bacteria gain access to the central nervous system (66). As the blood-brain endothelium has a high resistance to transport, it therefore appears that the *E. coli* K1 bacteria target a network of signalling molecules in order to stimulate macropinocytosis which the cell ordinarily uses as a broad and general mechanism for sampling fluid and solutes. By making use of the pleiotropic regulation of the host's macropinocytic machinery, the bacteria can thereby increase their own chances of uptake into the cells of the blood-brain barrier and thus invasion into the brain.

Materials and Methods

Cell culture and bacteria

Mammalian cells were maintained in a humidified 37°C, 5% CO_2 tissue culture incubator. Human brain microvascular endothelial cells (HBMEC) (67) were grown in RPMI-1640 supplemented with 20% (v/v) heat-inactivated foetal bovine serum (FBS) (Biosera, Ringmer, UK), 2 mM L-glutamine, 1 mM sodium pyruvate, 100 µg/ml streptomycin, 100 units/ml penicillin, non-essential amino acids (Gibco, Invitrogen, Paisley, UK), and vitamins (Gibco). Primary mouse lung endothelial cells (MLEC) (a kind gift from B.J. Nichols, MRC Laboratory of Molecular Biology, Cambridge, UK) were grown in 50:50 low glucose Dulbecco's Modified Eagles Medium (DMEM) and Ham's F12 supplemented with 20% (v/v) FBS, 0.00125% (w/v) heparin, 2 mM L-glutamine, 100 µg/ml streptomycin, and 100 units/ml penicillin, 0.1 mg/ml endothelial cell growth supplement (AbD Serotec, Oxford, UK). Reagents were purchased from Sigma-Aldrich (Poole, UK) unless otherwise stated.

Bacterial strains used were *E. coli* K1 (E44), which is a spontaneous rifampicin-resistant mutant of RS218 strain isolated from a neonatal meningitis patient (68), and *E. coli* HB101 (K-12), grown in Luria-Bertani (LB) broth at 37°C with shaking. *E. coli* K1 constitutively expressing mCherry (K1-Cherry) were described previously and are not compromised for invasion in HBMEC (69). *Listeria monocytogenes* (a kind gift from G. J. Bancroft, LSHTM) was grown in brain heart infusion (BHI) broth.

Antibodies

Antibodies used were: monoclonal mouse anti-β-actin (clone AC-15), monoclonal mouse anti-adaptin α (clone 8; BD Biosciences, Oxford, UK), monoclonal rabbit anti-pan Akt (Cell Signaling Technology, Danvers MA), polyclonal rabbit anti-phospho Akt (Ser473) (Cell Signaling Technology), polyclonal rabbit antibody to caveolin-1 (BD Biosciences), monoclonal mouse anti-clathrin (clone X22 was a kind gift from FM Brodsky, UCL) polyclonal rabbit anti-dynamin 2 (Genetex Inc. Irvine CA), polyclonal rabbit antibody to *E. coli* O18 (Mast Group, Bootle, UK), FluoProbes®-secondary antibodies (Interchim, Cheshire Science Ltd., Chester, UK), HRP-conjugated goat anti-mouse and HRP-conjugated goat anti-rabbit (Bio-Rad, Hemel-Hempstead, UK).

Gentamicin survival assay

HBMEC were grown to confluency in 24-well tissue culture plates, three wells for each condition. Experiments were conducted in low-serum media (RPMI-1640 supplemented with 5% FBS, and 2 mM L-glutamine), except where indicated. Cells were pretreated for 30 min with reagents and infected at multiplicity of infection (m.o.i.) of ~100 with mid-log phase *E. coli* K1, K1-Cherry or K-12, or with m.o.i. 10 with mid-log *L. monocytogenes,* as indicated. To facilitate bacterial association with cells, bacteria were centrifuged onto cells at 500 *g* for 5 min. Cells were infected for 1 hr at 37°C, unless indicated otherwise in the text, after which infected cells were overlaid with experimental media containing 100 µg/ml gentamicin for 1 hr at 37°C to kill extracellular bacteria. Cells were lysed with 0.3% (w/v) SDS in PBS to release *E. coli* or with 0.5% (w/v) saponin in PBS to release *L. monocytogenes*, and the number of viable bacteria released from the cells was assessed by bacterial colony-forming units (cfu) ascertained by titration on LB agar plates (or BHI agar plates for *L. monocytogenes*) and overnight incubation at 37°C. Results were expressed as the number of intracellular bacteria per cell relative to control. At least three independent experiments were undertaken.

Fluid phase and clathrin-mediated uptake assays

Alexa-Fluor® 647 transferrin (Molecular Probes, Invitrogen) or Alexa Fluor® 647 10 kD fixable dextran (Molecular Probes, Invitrogen) at final concentration of 25 µg/ml or 0.5 mg/ml, respectively were incubated with HBMEC for 30 min at 37°C, before washing at 4°C to arrest endocytosis. Transferrin-labelled cells were treated with an acid wash (0.5% acetic acid, 0.05 M NaCl, pH 3.0) for 2 min at 4°C to remove surface label and washed in RPMI to neutralise the acid. Cells were trypsinised, washed, and resuspended in FACS buffer (1% FCS in PBS).

Acquisition of flow cytometry data was performed on a BD™ LSRII (BD Biosciences, Oxford, UK) using appropriate laser lines, and analysed using FlowJo software (version 9, Tree Star, Ashland, OR, USA).

Pharmacological inhibitors

For cholesterol depletion or loading, cells were washed twice with RPMI (without serum, SFM) and pretreated at 37°C for 30 min with MβCD (methyl-β-cyclodextrin) or cholesterol-MβCD, respectively, in RPMI at a concentration range of 1-10 μM before addition of bacteria or labelled endocytic marker and assayed as described. For other chemical treatments, cells were pretreated with the reagent or control vehicle in experimental media for 30 min, prior to infection with *E. coli* K1 or labelled endocytic marker in the continuing presence of the reagent. Blebbistatin was used at 25-100 μM; chlorpromazine at 3-30 μM; cytochalasin D at 1-10 μM; dynasore at 80 μM or at concentration shown; EIPA at 80 μM; GF109203X at 25 μM; IPA-3 at 50 μM; jasplakinolide at 0.5-5 μM; nocodazole at 1 μg/ml; rottlerin at 50 μM; wortmannin at 10 μM. Reagents were tested for potential toxicity on HBMEC by trypan blue exclusion, and their effects on bacterial viability were tested by cfu analysis. Treatments with cholesterol-manipulating and macropinocytic inhibitory reagents were repeated with *L. monocytogenes* bacteria but the reagents were found to be bacteriostatic for this species and the results could not be interpreted.

Immunofluorescence and imaging

HBMEC were grown on 13 mm no. 1 glass coverslips (VWR, Lutterworth, UK) and infected as above with either *E. coli* K1 or K1-Cherry at moi ~100. Cells were fixed in 3% formaldehyde/PBS for 15 min at room temperature (RT), washed with PBS and then incubated for 10 min in 50 mM NH_4Cl in PBS. Cells were washed in 5% FCS/PBS (wash solution) and then were labelled sequentially with primary and secondary antibodies diluted in wash solution containing 0.2% saponin, each with 1 hr RT incubations. For actin staining, cells were labelled with phalloidin-TRITC at 10 μg/ml for 1 hr RT. For differential staining of intra- and extra-cellular bacteria, cells were initially stained with anti-*E. coli* O18 and then FluoProbes®-642 donkey anti-rabbit IgG without a permeabilisation agent, before proceeding to a second sequential staining step in the presence of saponin with anti-*E. coli* O18 and the related secondary tagged with another fluorophore (usually FluoProbes®-546) in combination with other antibodies as appropriate. Nuclei were stained with 1 μg/ml DAPI and cells were mounted onto a microscope slide with Confocal Matrix (Micro-Tech-Lab, Austria) or Fluoromount-G™ (eBioscience, Hatfield, UK).

To visualise dextran uptake with bacteria, cells were infected with mid-log *E. coli* K1 at moi ~100 in the presence of 500 μg/ml Alexa Fluor® 647 10 kD fixable dextran for 30 min, then fixed and stained for intra- and extracellular bacteria.

For transferrin uptake, Alexa Fluor® 555 transferrin (Gibco, Invitrogen) at 25 μg/ml was incubated for 30 min at 37°C with HBMEC transfected with dynamin 2-GFP plasmids, cells were fixed in 2% PFA and visualised.

Samples were observed with an inverted Zeiss LSM 510 confocal laser-scanning microscope (Carl Zeiss Ltd, Cambridge, UK) with appropriate lasers. To avoid potential experimental bias, tile z-stack images were acquired under software control. Images were processed with ImageJ (W. Rasband, National Institutes of Health, Bethesda, MD) and Adobe Photoshop.

Transient transfection of HBMEC

Plasmids encoding Dyn2(aa)WT-GFP and Dyn2(aa)K44A-GFP (37) were kind gifts from M.A. McNiven (Mayo Clinic, Rochester, MN, USA), Dyn1WT-GFP and Dyn1K44A-GFP were generously provided by H.T. McMahon (MRC LMB, Cambridge, UK), Cav1-GFP (70) was from B.J. Nichols (MRC LMB, Cambridge, UK), and the GFP-tagged caveolin-1 mutant constructs were kindly provided by M.O. Parat (University of Queensland, Australia) (71). RhoA-GFP plasmid constructs and pGFP wt Rac1 and pGFP L61 Rac1 were kind gifts from A.J. Ridley (King's College, London, UK) (72); pGFP-Rac1N17 from P. Fort (CNRS Montpellier, France) (73); cdc42-GFP constructs were from B.J. Nichols (74); Lifeact-GFP was from M. Parsons (75,76). pEGFP-N1 (Clontech, BD Biosciences) was used as the soluble GFP control and pLDLR A18 GFP, a kind gift from G.E. Kreitzer (University of Cornell, NY, USA) (77), as the membrane-bound GFP control.

For plasmid DNA transfection, HBMEC were seeded onto glass cover slips, grown to approximately 80% confluency, and were transfected using jetPRIME™ transfection reagent (Polyplus-transfection SA, Illkirch, France) according to the manufacturer's instructions. Approximately 20 hr post-transfection, cells were infected with K1-Cherry bacteria and imaged as described (69). Briefly, following infection as above, cells were incubated in experimental medium containing 100 μg/ml gentamicin at 37°C for 1 hr. Coverslips were washed and mounted onto a low-tech rubber gasket imaging chamber with approximately 35 μl imaging medium [RPMI-1640 without phenol red supplemented with 5% (v/v) FBS, 2 mM L-glutamine, 25 mM HEPES (pH 7.4)] (69,78). Live cells were held at 37°C on the microscope stage and tile z-stack images were acquired. Infection was quantified manually by counting the number of GFP positive cells with intracellular bacteria ($n \geq 30$ GFP-positive cells).

For live cell time series of *E. coli* K1 infection, K1-Cherry bacteria were centrifuged onto transfected HBMEC and cells were immediately transferred to the microscope stage and imaged continuously at 37°C for 1 hr. Images and movies were generated and analyzed using the Zeiss LSM software and ImageJ software.

siRNA transfection

Non-targeting siRNA or AP2A1, caveolin-1 and dynamin 2 siRNA (all SMARTpool siGENOME siRNA from Dharmacon, GE Healthcare) were delivered to cells at a final concentration of 50 μM,

using Lipofectamine RNAiMAX. Assays were carried out after 48 hr. Knockdown efficiency was ascertained by lysis of control cell wells in RIPA buffer (140 mM NaCl, 1 mM EDTA, 0.5 mM EGTA, 1% Triton X-100, 0.1% sodium deoxycholate, 0.1% SDS, 10 mM Tris, pH 8.0) supplemented with protease inhibitor cocktail (ThermoFisher Scientific, Waltham MA), followed by protein gel electrophoresis, Western blotting and detection of HRP-conjugated secondary antibodies with Pierce™ ECL Western Blotting Substrate (ThermoFisher Scientific).

Macropinocytosis assay

HBMEC were grown to confluency in 12-well plates, then incubated in experimental media for 1 hr prior to refreshment with experimental media supplemented with 200 µg/ml FITC-dextran (10 kD dextran conjugated to FITC) ± mid-log *E. coli* K1 at moi ~100 for 2 hr at 37°C. As a positive control HBMEC cells were incubated with experimental media containing 20% FCS and 200 µg/ml FITC-dextran (41). Following the infection period, cells were washed and incubated for 1 hr with fresh experimental media supplemented with 100 µg/ml gentamicin, after which they were washed, trypsinised, labelled with LIVE/DEAD® Fixable Near-IR stain (Molecular Probes, Invitrogen) and suspended in FACS buffer. Acquisition of flow cytometry data was performed as described above.

Actin quantitation

Images of serial sections of HBMEC stained with phalloidin were thresholded (Intermodes setting) and fluorescence area quantified in ImageJ. Quantitation of actin was applied to apical sections for the ruffling data.

Statistical analysis

All experiments were repeated three times and performed in duplicate or triplicate. GraphPad Prism Version 6 software was used for statistical analysis. For comparison of data from two experimental conditions, the two-tailed Student's *t* test was used to test statistical significance. For multiple comparisons, statistical significance was tested using one-way analysis of variance followed by the Newman-Keuls post-hoc test. A *p* value less than 0.05 was considered significant. In the figure legends, * $p<0.05$, ** $p<0.01$, *** $p<0.001$.

Acknowledgements

We gratefully thank all those that provided reagents used in this work – Dr B.J. Nichols for plasmids and primary MLEC cells, and Dr G. Otto for MLEC isolation. P. Fort, H.T. McMahon, M.A. McNiven, M.-O. Parat, G.E. Kreitzer, M. Parsons and A.J. Ridley kindly provided plasmids, F.M. Brodsky provided clathrin antibody, G.J. Bancroft provided the *Listeria* strain and N. Altan-Bonnet provided labelled transferrin. We also thank Andrea Zelmer and Nihal Altan-Bonnet for critical reading of this manuscript and Xufeng Wu (Light Microscopy Core, NHLBI) for assistance with image analysis. LNL was supported by a Bloomsbury Colleges PhD Studentship and the Central Research Fund, University of London.

References

1. Bonacorsi S, Bingen E. Molecular epidemiology of *Escherichia coli* causing neonatal meningitis. Int J Med Microbiol 2005;295:373-381.
2. de Louvois J, Halket S, Harvey D. Neonatal meningitis in England and Wales: sequelae at 5 years of age. Eur J Pediatr 2005;164:730-734.
3. Heath PT, Okike IO. Neonatal bacterial meningitis: an update. Paediatr Child Health 2010;20:526-530.
4. Okike IO, Johnson AP, Henderson KL, Blackburn RM, Muller-Pebody B, Ladhani SN, Anthony M, Ninis N, Heath PT. Incidence, etiology, and outcome of bacterial meningitis in infants aged <90 days in the United Kingdom and Republic of Ireland: prospective, enhanced, national population-based surveillance. Clin Infect Dis 2014;59:e150-e157.
5. May M, Daley AJ, Donath S, Isaacs D. Early onset neonatal meningitis in Australia and New Zealand, 1992-2002. Arch Dis Child Fetal Neonatal Ed 2005;90:F324-F327.
6. Wu J-H, Chen C-Y, Tsao P-N, Hsieh W-S, Chou H-C. Neonatal sepsis: a 6-year analysis in a neonatal care unit in Taiwan. Pediatr Neonatol 2009;50:88-95.
7. Furyk JS, Swann O, Molyneux E. Systematic review: neonatal meningitis in the developing world. Trop Med Int Health 2011;16:672-679.
8. Stoll BJ, Hansen NI, Sánchez PJ, Faix RG, Poindexter BB, Van Meurs KP, Bizzarro MJ, Goldberg RN, Frantz ID, III, Hale EC, Shankaran S, Kennedy K, Carlo WA, Watterberg KL, Bell EF, *et al.* Early onset neonatal sepsis: the burden of group B Streptococcal and *E. coli* disease continues. Pediatrics 2011;127:817-826.
9. Kim KS. Current concepts on the pathogenesis of *Escherichia coli* meningitis: implications for therapy and prevention. Curr Opin Infect Dis 2012;25:273-278.
10. Reddy MA, Prasadarao NV, Wass CA, Kim KS. Phosphatidylinositol 3-kinase activation and interaction with focal adhesion kinase in *Escherichia coli* K1 invasion of human brain microvascular endothelial cells. J Biol Chem 2000;275:36769-36774.
11. Reddy MA, Wass CA, Kim KS, Schlaepfer DD, Prasadarao NV. Involvement of focal adhesion kinase in *Escherichia coli* invasion of human brain microvascular endothelial cells. Infect Immun 2000;68:6423-6430.
12. Khan NA, Wang Y, Kim KJ, Chung JW, Wass CA, Kim KS. Cytotoxic necrotizing factor-1 contributes to *Escherichia coli K1* invasion of the central nervous system. J Biol Chem 2002;277:15607-15612.
13. Prasadarao NV. Identification of *Escherichia coli* outer membrane protein A receptor on human brain microvascular endothelial cells. Infect Immun 2002;70:4556-4563.
14. Khan NA, Shin S, Chung JW, Kim KJ, Elliott S, Wang Y, Kim KS. Outer membrane protein A and cytotoxic necrotizing factor-1 use diverse signaling mechanisms for *Escherichia coli* K1 invasion of human brain microvascular endothelial cells. Microb Pathog 2003;35:35-42.

15. Rudrabhatla RS, Selvaraj SK, Prasadarao NV. Role of Rac1 in *Escherichia coli* K1 invasion of human brain microvascular endothelial cells. Microbes Infect 2006;8:460-469.
16. Maruvada R, Argon Y, Prasadarao NV. *Escherichia coli* interaction with human brain microvascular endothelial cells induces signal transducer and activator of transcription 3 association with the C-terminal domain of Ec-gp96, the outer membrane protein A receptor for invasion. Cell Microbiol 2008;10:2326-2338.
17. Maruvada R, Kim KS. IbeA and OmpA of *Escherichia coli* K1 exploit Rac1 activation for invasion of human brain microvascular endothelial cells. Infect Immun 2012;80:2035-2041.
18. Prasadarao NV, Wass CA, Stins MF, Shimada H, Kim KS. Outer membrane protein A-promoted actin condensation of brain microvascular endothelial cells is required for *Escherichia coli* invasion. Infect Immun 1999;67:5775-5783.
19. Kumari S, Swetha MG, Mayor S. Endocytosis unplugged: multiple ways to enter the cell. Cell Res 2010;20:256-275.
20. Kühling L, Schelhaas M. Systematic analysis of endocytosis by cellular perturbations. Methods Mol Biol 2014;1174:19-46.
21. Sukumaran SK, Quon MJ, Prasadarao NV. *Escherichia coli* K1 internalization via caveolae requires caveolin-1 and protein kinase Cα interaction in human brain microvascular endothelial cells. J Biol Chem 2002;277:50716-50724.
22. Chi F, Jong TD, Wang L, Ouyang Y, Wu C, Li W, Huang S-H. Vimentin-mediated signalling is required for IbeA+ *E. coli* K1 invasion of human brain microvascular endothelial cells. Biochem J 2010;427:79-90.
23. Mercer J, Helenius A. Virus entry by macropinocytosis. Nat Cell Biol 2009;11:510-520.
24. Schnitzer JE, Oh P, Pinney E, Allard J. Filipin-sensitive caveolae-mediated transport in endothelium: reduced transcytosis, scavenger endocytosis, and capillary permeability of select macromolecules. J Cell Biol 1994;127:1217-1232.
25. Orlandi PA, Fishman PH. Filipin-dependent inhibition of cholera toxin: evidence for toxin internalization and activation through caveolae-like domains. J Cell Biol 1998;141:905-915.
26. Grimmer S, van Deurs B, Sandvig K. Membrane ruffling and macropinocytosis in A431 cells require cholesterol. J Cell Sci 2002;115:2953-2962.
27. Anderson HA, Chen Y, Norkin LC. Bound simian virus 40 translocates to caveolin-enriched membrane domains, and its entry is inhibited by drugs that selectively disrupt caveolae. Mol Biol Cell 1996;7:1825-1834.
28. Hu G, Schwartz DE, Shajahan AN, Visintine DJ, Salem MR, Crystal GJ, Albrecht RF, Vogel SM, Minshall RD. Isoflurane, but not sevoflurane, increases transendothelial albumin permeability in the isolated rat lung. Role for enhanced phosphorylation of caveolin-1. Anesthesiology 2006;104:777-785.
29. Watson RO, Galán JE. *Campylobacter jejuni* survives within epithelial cells by avoiding delivery to lysosomes. PLoS Pathog 2008;4:e14.
30. Mora R, Bonilha VL, Marmorstein A, Scherer PE, Brown D, Lisanti MP, Rodriguez-Boulan E. Caveolin-2 localizes to the Golgi complex but redistributes to plasma membrane, caveolae, and rafts when co-expressed with caveolin-1. J Biol Chem 1999;274:25708-25717.
31. Parolini I, Sargiacomo M, Galbiati F, Rizzo G, Grignani F, Engelman JA, Okamoto T, Ikezu T, Scherer PE, Mora R, Rodriguez-Boulan E, Peschle C, Lisanti MP. Expression of caveolin-1 is required for the transport of caveolin-2 to the plasma membrane. Retention of caveolin-2 at the level of the Golgi complex. J Biol Chem 1999;274:25718-25725.
32. Drab M, Verkade P, Elger M, Kasper M, Lohn M, Lauterbach B, Menne J, Lindschau C, Mende F, Luft FC, Schedl A, Haller H, Kurzchalia TV. Loss of caveolae, vascular dysfunction, and pulmonary defects in caveolin-1 gene-disrupted mice. Science 2001;293:2449-2452.
33. Razani B, Engelman JA, Wang XB, Schubert W, Zhang XL, Marks CB, Macaluso F, Russell RG, Li M, Pestell RG, Di Vizio D, Hou H, Jr., Kneitz B, Lagaud G, Christ GJ*, et al.* Caveolin-1 null mice are viable but show evidence of hyperproliferative and vascular abnormalities. J Biol Chem 2001;276:38121-38138.
34. Oh P, McIntosh DP, Schnitzer JE. Dynamin at the neck of caveolae mediates their budding to form transport vesicles by GTP-driven fission from the plasma membrane of endothelium. J Cell Biol 1998;141:101-114.
35. Shajahan AN, Timblin BK, Sandoval R, Tiruppathi C, Malik AB, Minshall RD. Role of *Src*-induced dynamin-2 phosphorylation in caveolae-mediated endocytosis in endothelial cells. J Biol Chem 2004;279:20392-20400.
36. Yao Q, Chen J, Cao H, Orth JD, McCaffery JM, Stan R-V, McNiven MA. Caveolin-1 interacts directly with dynamin-2. J Mol Biol 2005;348:491-501.
37. Cao H, Garcia F, McNiven MA. Differential distribution of dynamin isoforms in mammalian cells. Mol Biol Cell 1998;9:2595-2609.
38. Veiga E, Cossart P. *Listeria* hijacks the clathrin-dependent endocytic machinery to invade mammalian cells. Nat Cell Biol 2005;7:894-900.
39. Park RJ, Shen H, Liu L, Liu X, Ferguson SM, De Camilli P. Dynamin triple knockout cells reveal off target effects of commonly used dynamin inhibitors. J Cell Sci 2013;126:5305-5312.
40. Cao H, Chen J, Awoniyi M, Henley JR, McNiven MA. Dynamin 2 mediates fluid-phase micropinocytosis in epithelial cells. J Cell Sci 2007;120:4167-4177.
41. Krzyzaniak MA, Zumstein MT, Gerez JA, Picotti P, Helenius A. Host cell entry of respiratory syncytial virus involves macropinocytosis followed by proteolytic activation of the F protein. PLoS Pathog 2013;9:e1003309.
42. Koivusalo M, Welch C, Hayashi H, Scott CC, Kim M, Alexander T, Touret N, Hahn KM, Grinstein S. Amiloride inhibits macropinocytosis by lowering submembranous pH and preventing Rac1 and Cdc42 signaling. J Cell Biol 2010;188:547-563.
43. Sandgren KJ, Wilkinson J, Miranda-Saksena M, McInerney GM, Byth-Wilson K, Robinson PJ,

Cunningham AL. A differential role for macropinocytosis in mediating entry of the two forms of vaccinia virus into dendritic cells. PLoS Pathog 2010;6:e1000866.
44. Ivanov AI. Pharmacological inhibition of endocytic pathways: is it specific enough to be useful? Methods Mol Biol 2008;440:15-33.
45. Vercauteren D, Vandenbroucke RE, Jones AT, Rejman J, Demeester J, De Smedt SC, Sanders NN, Braeckmans K. The use of inhibitors to study endocytic pathways of gene carriers: optimization and pitfalls. Mol Ther 2010;18:561-569.
46. Daniel JA, Chau N, Abdel-Hamid MK, Hu L, von Kleist L, Whiting A, Krishnan S, Maamary P, Joseph SR, Simpson F, Haucke V, McCluskey A, Robinson PJ. Phenothiazine-derived antipsychotic drugs inhibit dynamin and clathrin-mediated endocytosis. Traffic 2015;16:635-654.
47. Bonazzi M, Vasudevan L, Mallet A, Sachse M, Sartori A, Prevost M-C, Roberts A, Taner SB, Wilbur JD, Brodsky FM, Cossart P. Clathrin phosphorylation is required for actin recruitment at sites of bacterial adhesion and internalization. J Cell Biol 2011;195:525-536.
48. Dutta D, Donaldson JG. Sorting of clathrin-independent cargo proteins depends on Rab35 delivered by clathrin-mediated endocytosis. Traffic 2015;16:994-1009.
49. Rubin LL, Staddon JM. The cell biology of the blood-brain barrier. Annu Rev Neurosci 1999;22:11-28.
50. Fiorentini C, Falzano L, Fabbri A, Stringaro A, Logozzi M, Travaglione S, Contamin S, Arancia G, Malorni W, Fais S. Activation of Rho GTPases by cytotoxic necrotizing factor 1 induces macropinocytosis and scavenging activity in epithelial cells. Mol Biol Cell 2001;12:2061-2073.
51. Fabbri A, Falzano L, Travaglione S, Stringaro A, Malorni W, Fais S, Fiorentini C. Rho-activating *Escherichia coli* cytotoxic necrotizing factor 1: macropinocytosis of apoptotic bodies in human epithelial cells. Int J Med Microbiol 2002;291:551-554.
52. Higuchi M, Onishi K, Kikuchi C, Gotoh Y. Scaffolding function of PAK in the PDK1–Akt pathway. Nat Cell Biol 2008;10:1356-1364.
53. Ju R, Simons M. Syndecan 4 regulation of PDK1-dependent Akt activation. Cell Signal 2013;25:101-105.
54. Mercer J, Helenius A. Gulping rather than sipping: macropinocytosis as a way of virus entry. Current opinion in microbiology 2012;15:490-499.
55. Patel JC, Galán JE. Differential activation and function of Rho GTPases during *Salmonella*-host cell interactions. J Cell Biol 2006;175:453-463.
56. Swanson JA. Shaping cups into phagosomes and macropinosomes. Nat Rev Mol Cell Biol 2008;9:639-649.
57. Mercer J, Helenius A. Apoptotic mimicry: phosphatidylserine-mediated macropinocytosis of vaccinia virus. Ann N Y Acad Sci 2010;1209:49-55.
58. Mercer J, Knébel S, Schmidt FI, Crouse J, Burkard C, Helenius A. Vaccinia virus strains use distinct forms of macropinocytosis for host-cell entry. Proc Natl Acad Sci USA 2010;107:9346-9351.
59. Parton RG, Simons K. The multiple faces of caveolae. Nat Rev Mol Cell Biol 2007;8:185-194.
60. Cheng JPX, Nichols BJ. Caveolae: One function or many? Trends Cell Biol 2016;26:177-189.
61. Le Lay S, Li Q, Proschogo N, Rodriguez M, Gunaratnam K, Cartland S, Rentero C, Jessup W, Mitchell T, Gaus K. Caveolin-1-dependent and -independent membrane domains. J Lipid Res 2009;50:1609-1620.
62. Ariotti N, Fernández-Rojo MA, Zhou Y, Hill MM, Rodkey TL, Inder KL, Tanner LB, Wenk MR, Hancock JF, Parton RG. Caveolae regulate the nanoscale organization of the plasma membrane to remotely control Ras signaling. J Cell Biol 2014;204:777-792.
63. Chaudhary N, Gomez GA, Howes MT, Lo HP, McMahon K-A, Rae JA, Schieber NL, Hill MM, Gaus K, Yap AS, Parton RG. Endocytic crosstalk: cavins, caveolins, and caveolae regulate clathrin-independent endocytosis. PLoS Biol 2014;12:e1001832.
64. Hoffmann C, Berking A, Agerer F, Buntru A, Neske F, Chhatwal GS, Ohlsen K, Hauck CR. Caveolin limits membrane microdomain mobility and integrin-mediated uptake of fibronectin-binding pathogens. J Cell Sci 2010;123:4280-4291.
65. Preta G, Cronin JG, Sheldon IM. Dynasore - not just a dynamin inhibitor. Cell Commun Signal 2015;13:24.
66. Zelmer A, Bowen M, Jokilammi A, Finne J, Luzio JP, Taylor PW. Differential expression of the polysialyl capsule during blood-to-brain transit of neuropathogenic *Escherichia coli* K1. Microbiology 2008;154:2522-2532.
67. Stins MF, Badger J, Sik Kim K. Bacterial invasion and transcytosis in transfected human brain microvascular endothelial cells. Microb Pathog 2001;30:19-28.
68. Achtman M, Mercer A, Kusecek B, Pohl A, Heuzenroeder M, Aaronson W, Sutton A, Silver RP. Six widespread bacterial clones among *Escherichia coli* K1 isolates. Infect Immun 1983;39:315-335.
69. Loh LN, Ward TH. *Escherichia coli* K1 invasion of human brain microvascular endothelial cells. Methods Enzymol 2012;506:93-113.
70. Pelkmans L, Kartenbeck J, Helenius A. Caveolar endocytosis of simian virus 40 reveals a new two-step vesicular-transport pathway to the ER. Nat Cell Biol 2001;3:473-483.
71. Parat M-O, Anand-Apte B, Fox PL. Differential caveolin-1 polarization in endothelial cells during migration in two and three dimensions. Mol Biol Cell 2003;14:3156-3168.
72. Hall A. Rho GTPases and the actin cytoskeleton. Science 1998;279:509-514.
73. Blangy A, Vignal E, Schmidt S, Debant A, Gauthier-Rouvière C, Fort P. TrioGEF1 controls Rac- and Cdc42-dependent cell structures through the direct activation of rhoG. J Cell Sci 2000;113:729-739.
74. Sabharanjak S, Sharma P, Parton RG, Mayor S. GPI-anchored proteins are delivered to recycling endosomes via a distinct cdc42-regulated, clathrin-independent pinocytic pathway. Dev Cell 2002;2:411-423.

75. Riedl J, Crevenna AH, Kessenbrock K, Yu JH, Neukirchen D, Bista M, Bradke F, Jenne D, Holak TA, Werb Z, Sixt M, Wedlich-Soldner R. Lifeact: a versatile marker to visualize F-actin. Nat Methods 2008;5:605-607.
76. Costa P, Scales TME, Ivaska J, Parsons M. Integrin-specific control of focal adhesion kinase and RhoA regulates membrane protrusion and invasion. PLoS One 2013;8:e74659.
77. Kreitzer G, Schmoranzer J, Low SH, Li X, Gan Y, Weimbs T, Simon SM, Rodriguez-Boulan E. Three-dimensional analysis of post-Golgi carrier exocytosis in epithelial cells. Nat Cell Biol 2003;5:126-136.
78. Ward TH. Trafficking through the early secretory pathway of mammalian cells. In: van der Giezen M, editor. Protein Targeting Protocols. 2nd ed. New Jersey: Humana Press; 2007. p. 281-296.

Figure Legends

Figure 1. *E. coli* K1 recruits actin to invade HBMEC. **A-D.** HBMEC cells were infected with *E. coli* K1 for 30 min, fixed and stained with differential permeabilisation for bacteria and actin. External bacteria are shown in purple, bacteria that stained only after permeabilisation (i.e. internalised bacteria) are blue, actin in green. Scale bar 5 μm. **A.** Projected z stack of group of cells, shown in **B** at higher magnification from a single confocal slice in xy and xz dimensions. Note actin cup (yellow arrowhead) around central bacterium. **C.** Internalised bacteria (white arrowhead) surrounded by actin (yellow arrowhead), **D.** Internalised bacteria (white arrowhead) no longer colocalising with actin. **E.** Cells were pretreated with cytoskeleton-disrupting agents for 30 min, then infected with *E. coli* K1 for 1 hr. Internalised bacteria were assayed by colony counting and normalised to the appropriate mock treatment, either RPMI alone or with DMSO. Cyt D, cytochalasin D; Jasp, jasplakinolide; Bleb, blebbistatin; NZ, nocodazole; concentrations as shown. Data shown are mean ± SEM from two independent experiments with three replicates each. *** $p<0.001$ compared to related mock treatment.

Figure 2. Rho family GTPases alter *E. coli* K1 invasion dynamics and are recruited onto bacterial vacuoles. A. Graphs showing quantitation of GFP-GTPase-expressing HBMEC containing intracellular bacteria following 2 hr infection at moi ~100. In each graph, the data is normalised to the transfection control cells expressing GFP only in the left column, then the columns in order indicate data from cells expressing the GFP-tagged wild type (WT) GTPase, those expressing the dominant positive mutant and the right column the dominant negative GTPase. Cells expressing dominant positive Rho GTPases show a significant increase in number of infected mutant-expressing cells, while cells expressing the inactive mutant of Rac1 and RhoA show an inhibition in bacterial invasion as compared to the GFP control. Data shown are mean ± SEM of 3 independent experiments normalised to soluble GFP transfection control. No significant difference was found in number of intracellular bacteria per cell. **B** shows xy view of cell containing intracellular bacteria either enclosed in a cdc42-labelled vacuole (white arrow) or without cdc42 label (yellow arrowhead). **C** shows the corresponding orthogonal view. **D** The effect of kinase inhibitors (IPA-3, GF109203X, wortmannin) on *E. coli* K1 infection (1 hr) and on uptake of transferrin and dextran markers (30 min) was assayed by colony counting and by flow cytometry, respectively, and normalised to the control. Data shown are mean ± SEM of 2 independent experiments each with triplicate samples. # data not shown owing to overlapping emission spectra of kinase inhibitor and fluorescent marker. *** $p<0.001$

Figure 3. *E. coli* K1 invasion of HBMEC is inhibited upon cholesterol depletion. A. HBMEC cells were pretreated with methyl-β-cyclodextrin (MbCD) or loaded with cholesterol at indicated concentrations 30 min before infection with *E. coli* K1 for 1 hr. Internalised bacteria were assayed by colony counting and normalised to control treatment (SFM). **B.** HBMEC cells were pretreated as in **A**, then labelled with FITC-dextran and transferrin-Alexa Fluor 647 for 30 min at 37°C. 10,000 cells were analysed by flow cytometry and normalised to untreated cells. Data shown are mean ± SEM from two independent experiments with three replicates each. * $p<0.05$, ** $p<0.01$, *** $p<0.001$

Figure 4. Manipulation of caveolae function does not alter *E. coli* K1 invasion. A. Confocal image of intracellular bacterium associated with caveolin-1 following infection with *E. coli* K1 for 30 min and cell fixation. DAPI labels DNA in the host cell and the bacteria. Arrow indicates association of caveolin-1 around invading bacteria while arrowheads indicate bacteria without specific caveolin-1 association. Scale bar 5 μm. **B**. Quantification from micrographs of intracellular bacteria associated with caveolin-1 following infection for the time indicated. A decrease in the percentage of bacteria associated with caveolin-1 was observed, although very few bacteria are associated with caveolin-1 even at the earliest timepoint. **C.** GFP-tagged caveolin-1 mutant constructs inhibit caveolae-dependent uptake of cargo or bacteria. HBMEC cells were transiently transfected with caveolin-1-GFP chimaeras: wild type (WT) or phosphorylation mutant (Tyr14) as indicated. LDLR A18 GFP was a transfection control. GFP-expressing cells were scored for the presence of intracellular *E. coli* K1 following infection for 2 hr. There was no statistically significant difference seen in bacterial invasion between cells expressing caveolin-1 WT and caveolin-1 Tyr14 (or other caveolin-1 mutants, not shown). **D**. Mouse lung endothelial cells (MLEC) isolated from wild type and caveolin-1 knockout mice were infected with either *E. coli* K1 or non-pathogenic *E. coli* K-12 for 2 hr, then bacterial invasion analysed by cfu assay. **E.** Uptake of *E. coli* K1 for 2 hr following siRNA depletion of caveolin-1. Protein expression was quantitated by Western blotting of samples and relative expression determined against negative siRNA (data not shown). Actin was used as a loading control. Data shown are mean ± SD of 2 or 3 independent experiments each with triplicate samples. * $p<0.05$

Figure 5. Manipulation of dynamin activity inhibits bacterial invasion of HBMEC. A. HBMEC cells transiently transfected with GFP-tagged dynamin constructs were infected with K1-Cherry for 2 hr. GFP-expressing cells were scored for the presence of intracellular *E. coli* K1. Soluble GFP was an experimental control. No statistically significant difference was seen between control, wild type and mutant dynamin, indicating that overexpression of dominant negative dynamin 1 and 2 did not inhibit *E. coli* K1 invasion of HBMEC. **B.** As for **A**, following infection with *L. monocytogenes*. **C.** HBMEC cells were pretreated for 30 min with dynasore at concentrations shown, then infected with either *E. coli* K1 or *L. monocytogenes* for 1 hr. Internalised bacteria were assayed by colony counting and normalised to the appropriate control (RPMI with DMSO). **D.** Uptake of *E. coli* K1 for 2 hr following siRNA depletion of dynamin 2. Protein expression was quantitated by Western blotting of samples and relative expression determined against negative siRNA (data not shown). Actin was used as a loading control. Data

shown are mean ± SEM of 2 or 3 independent experiments each with triplicate samples. * $p<0.05$, ** $p<0.01$, *** $p<0.001$

Figure 6. Macropinocytic uptake of *E. coli* K1. A. HBMEC cells were labelled with FITC-dextran in either experimental medium (low serum) or experimental medium supplemented with 20% serum (high serum) or infected with *E. coli* K1 in low serum experimental medium for 2 hr at 37°C. Cells were then analysed by flow cytometry for uptake of FITC dextran. Data shown are mean of triplicates ± SEM of one representative experiment. *P* values are from pairwise statistical analysis of 3 independent experiments. **B**. The effect of macropinocytosis inhibitors (EIPA and rottlerin) on 1 hr infection of HBMEC by *E. coli* K1 and on 30 min uptake of transferrin and dextran markers was assayed by colony counting and by flow cytometry, respectively, and normalised to the DMSO control. Data shown are mean ± SEM of 2 or 3 independent experiments each with triplicate samples. **C**. Confocal micrograph shows that intracellular bacteria colocalise with Alexa Fluor 647-dextran (white arrow) following 30 min infection of *E. coli* K1 while extracellular bacteria (yellow arrowhead) do not. Inset shows the corresponding orthoganol view of the internalised bacterium. **D**. Quantification of internalised bacteria colocalising with dextran as in **C**. Data shown are mean ± SEM from two independent experiments.

Figure 7. Effect of inhibition of clathrin-mediated endocytosis on *E. coli* K1 invasion. A. Uptake of *L. monocytogenes* and *E. coli* K1 for 1 hr, following pretreatment of HBMEC with the indicated concentrations of chlorpromazine (CPZ) for 30 min, was assayed by colony counting and normalised to the RPMI control. ** $p<0.01$, *** $p<0.001$ **B.** HBMEC cells transfected with siRNA as indicated were infected with *E. coli* K1 for 2 hr following pretreatment for 30 min with EIPA or with DMSO as a control and assayed by colony counting. Average AP2 knockdown was 76% ± 1%. Data shown are mean ± SEM of 2 independent experiments each with triplicate samples. **C.** Cells transfected with siRNA were infected with *E. coli* K1 for 30 min or 120 min (control was uninfected). Western blot of cell extracts shows total and phosphorylated Akt, AP2 and actin loading control for one experiment. Average AP2 knockdown was 83% ± 2.8%. **D.** Phosphorylated Akt relative to total Akt was quantified for 3 independent experiments. Data shown are mean ± SEM.

Figure 8. Model for *E. coli* K1 internalisation in HBMEC. *E. coli* K1 enter cells through an actin-dependent, cholesterol-dependent process, involving activation of Rho GTPase signalling pathways. Clathrin-mediated endocytosis may contribute indirectly through the uptake of LDL-derived cholesterol, or through control of receptor cycling.

Supplementary Information

Movie S1. Timelapse movie of actin in HBMEC in response to *E. coli* K1 infection. Cells expressing Lifeact-GFP (green) were infected with K1-mCherry at moi ~100. There is approx. 5 min time lag between centrifugation of bacteria onto cells and initiation of imaging. Images were captured at 27 sec intervals. Arrows indicate example cells where actin-based membrane ruffling was induced.

Movie S2. Timelapse movie S1 also showing K1-mCherry (red).

Figure S1. *E. coli* K1 induces membrane ruffling in HBMEC. A. Stills from timelapse Movie S1 (upper panel) and S2 (lower panel) at the times shown, demonstrating cells with increased actin ruffling at the plasma membrane (arrows). The area in the white square is enlarged in **B** to show an internalised bacterium remaining stationary inside the cell over time. At the end of the time series the internalised bacterium can be seen clearly in the orthogonal section (z view). **C.** Number of internalised bacteria associated with actin at given timepoints after infection quantified from data as in Figure 1. **D.** Cells were infected with either *E. coli* K1 or non-pathogenic *E. coli* K-12 strains for 15 min, fixed and stained for actin. Actin in apical sections (excluding stress fibres) was quantitated in ImageJ. Data shown are mean ± SEM of 2 independent experiments.

Figure S2. Transferrin uptake into HBMEC is inhibited by mutant dynamin expression while *E. coli* K1 shows no colocalisation with dynamin. A. HBMEC cells were transiently transfected with dynamin constructs, then labelled with transferrin-Alexa Fluor 555. Transferrin uptake was imaged after 30 min. In cells transfected with the Dyn2(aa)K44A construct, transferrin uptake is inhibited (GFP cells are outlined in the transferrin images). Scale bar 5 µm. **B**. Transferrin uptake was quantitated as total fluorescence per cell in GFP-positive cells, normalised to cells expressing the wild type construct. Data shown are mean ± SEM of 2 independent experiments. **C.** HBMEC cells were transiently transfected with GFP-tagged dynamin constructs, then infected with K1-Cherry for 2 hr. The confocal micrographs show adherent and internalised bacteria, as indicated, in cells expressing Dyn2(aa)WT-GFP both in the xy plane and the orthogonal section. Concentration of dynamin 2 is not observed around invading bacteria. External and internalised bacteria denoted by yellow and white arrowheads, respectively. Scale bar 5 µm.

Figure S3. Transferrin uptake into HBMEC is inhibited by CME inhibitors while *E. coli* K1 shows no colocalisation with clathrin. A. Uptake of transferrin and dextran markers was assayed by flow cytometry following pretreatment of HBMEC with either 30 µM CPZ or 80 µM dynasore and normalised to the RPMI or DMSO control, respectively. Data shown are mean ± SEM of 3 independent experiments each with duplicate samples. * $p<0.05$, *** $p<0.001$ **B.** HBMEC cells were infected with *L. monocytogenes* or *E. coli* K1 for 30 min, then fixed and stained for internalised bacteria and clathrin.

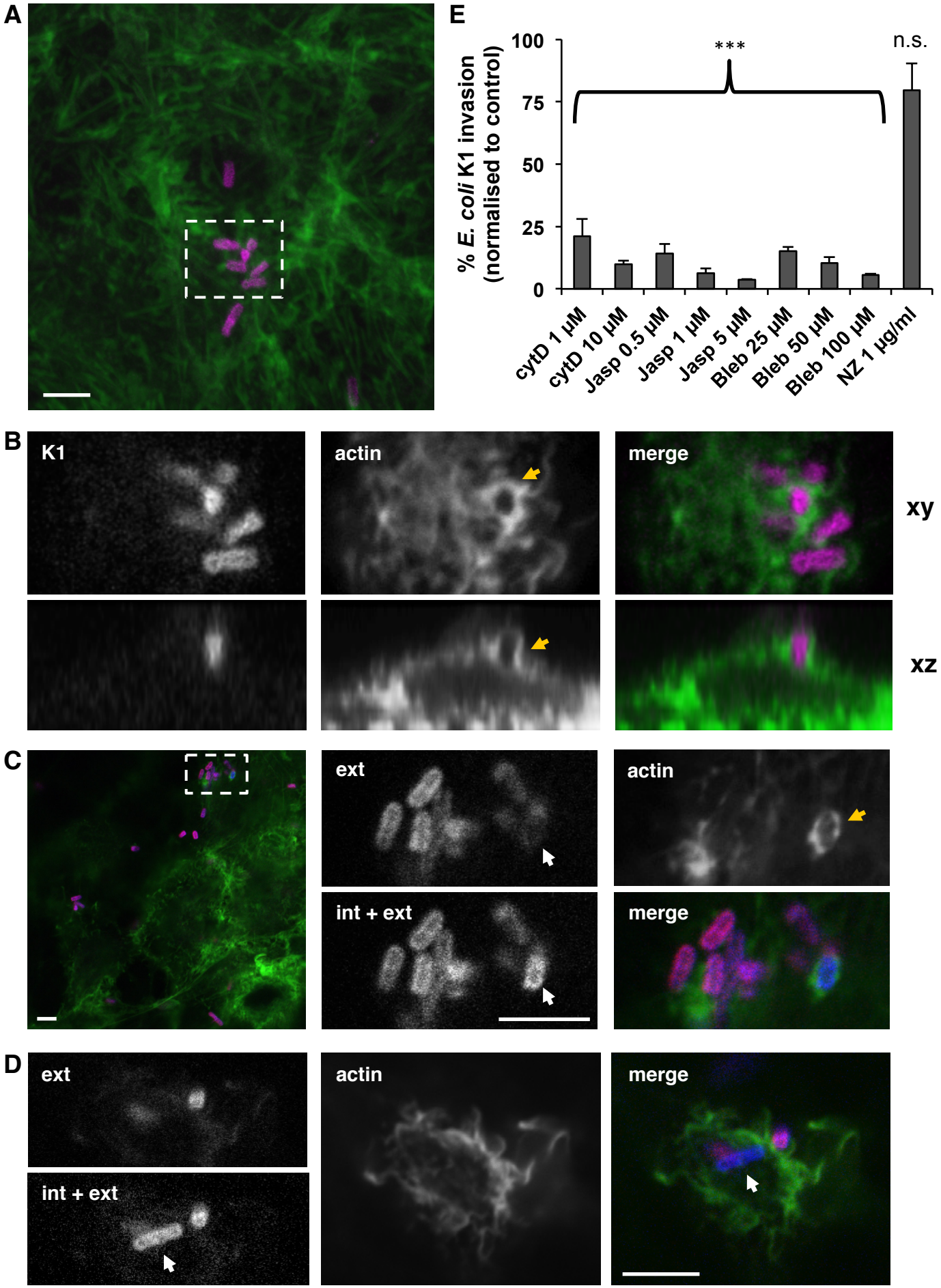

Loh et al Figure 1

Loh et al Figure 2

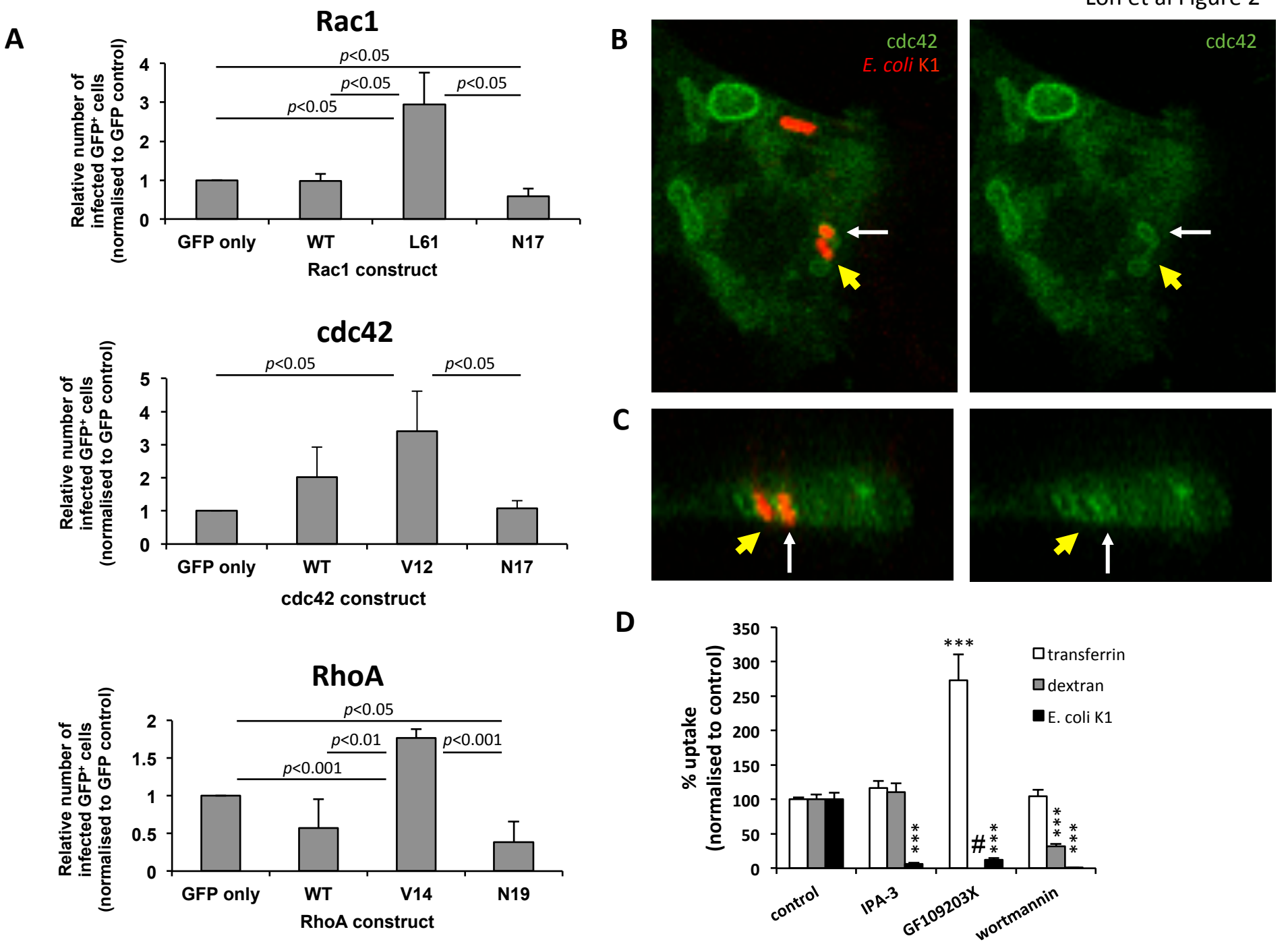

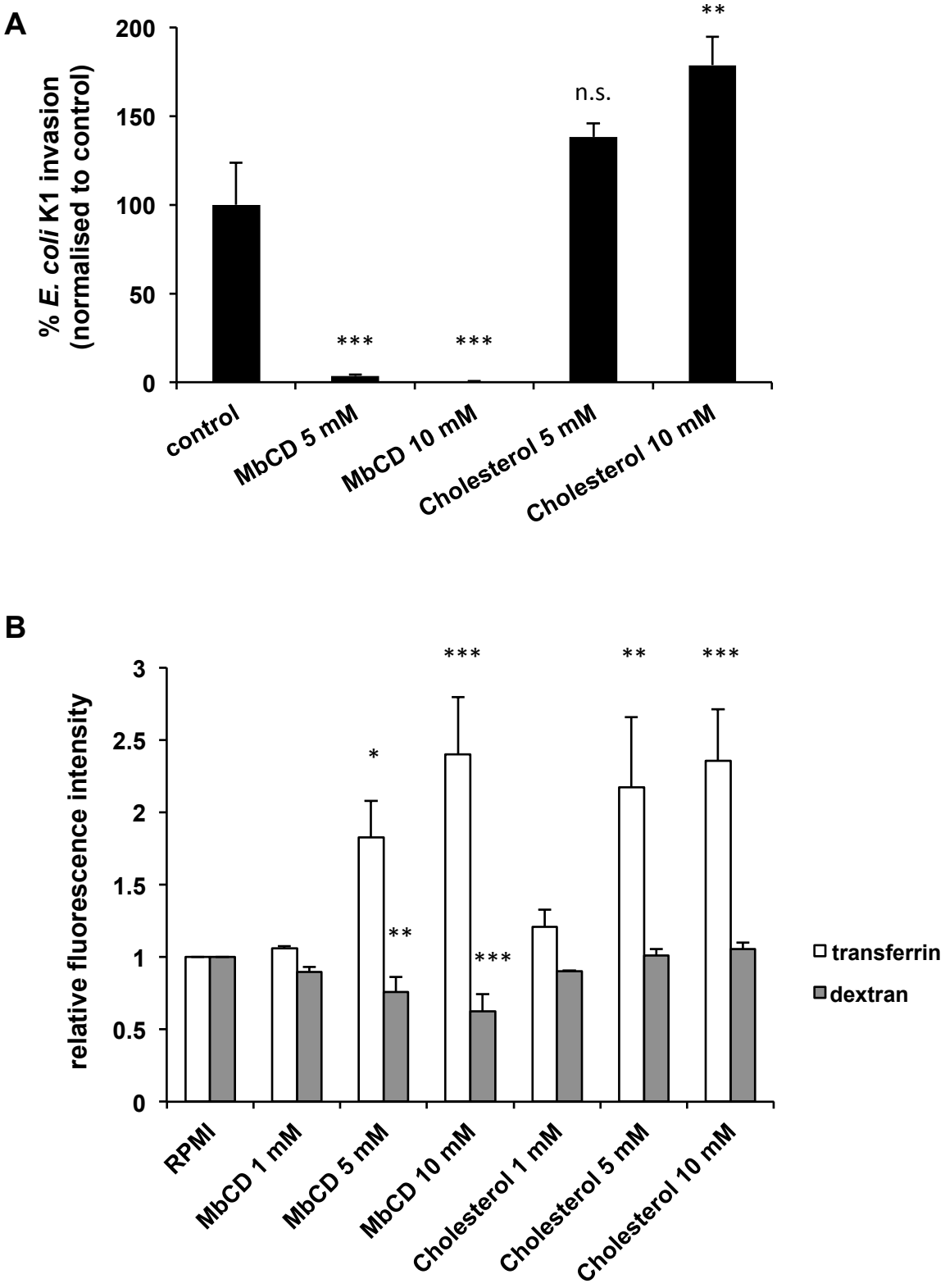

Loh et al Figure 3

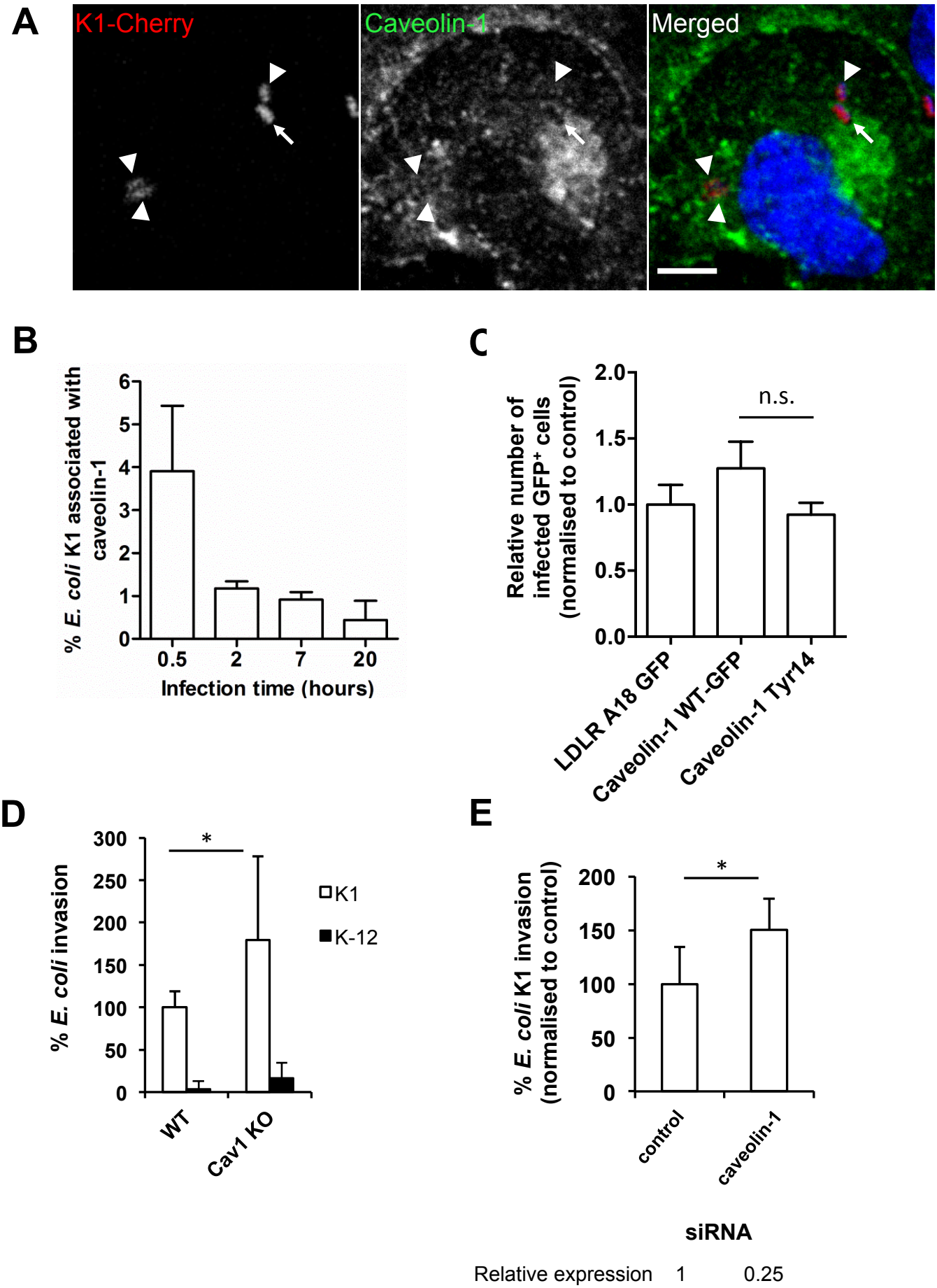

Loh et al Figure 4

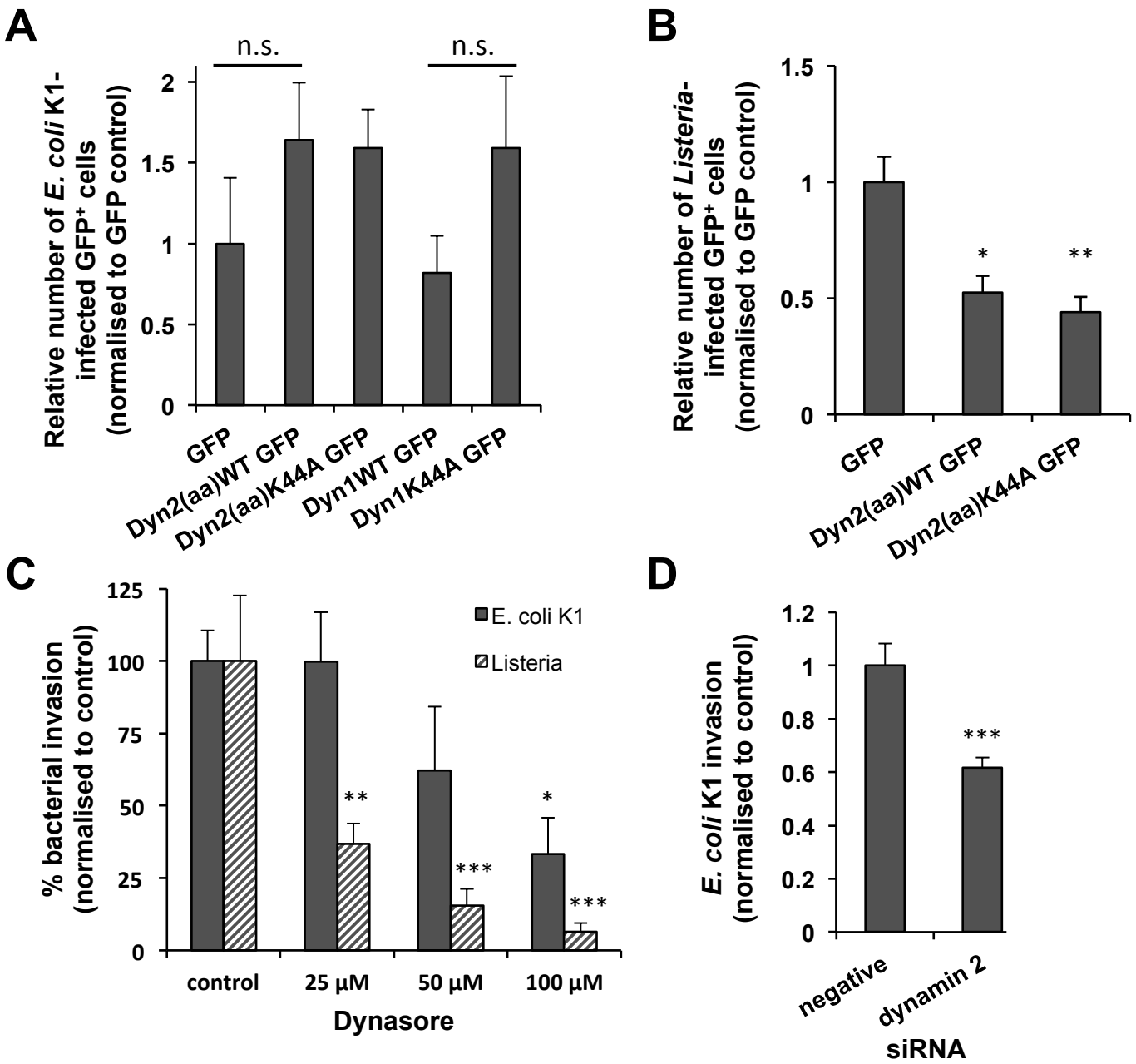

Loh et al Figure 5

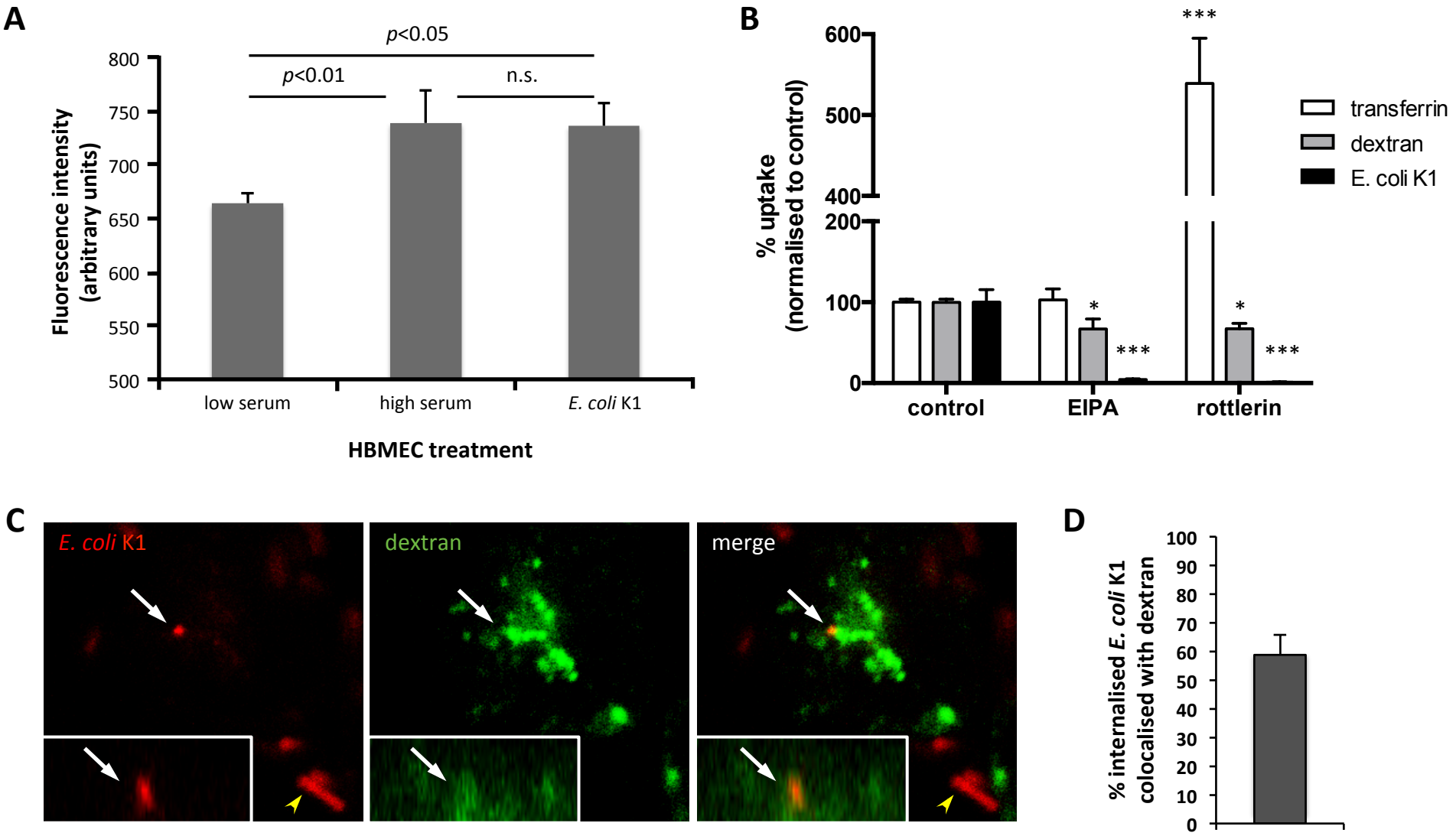

Loh et al Figure 6

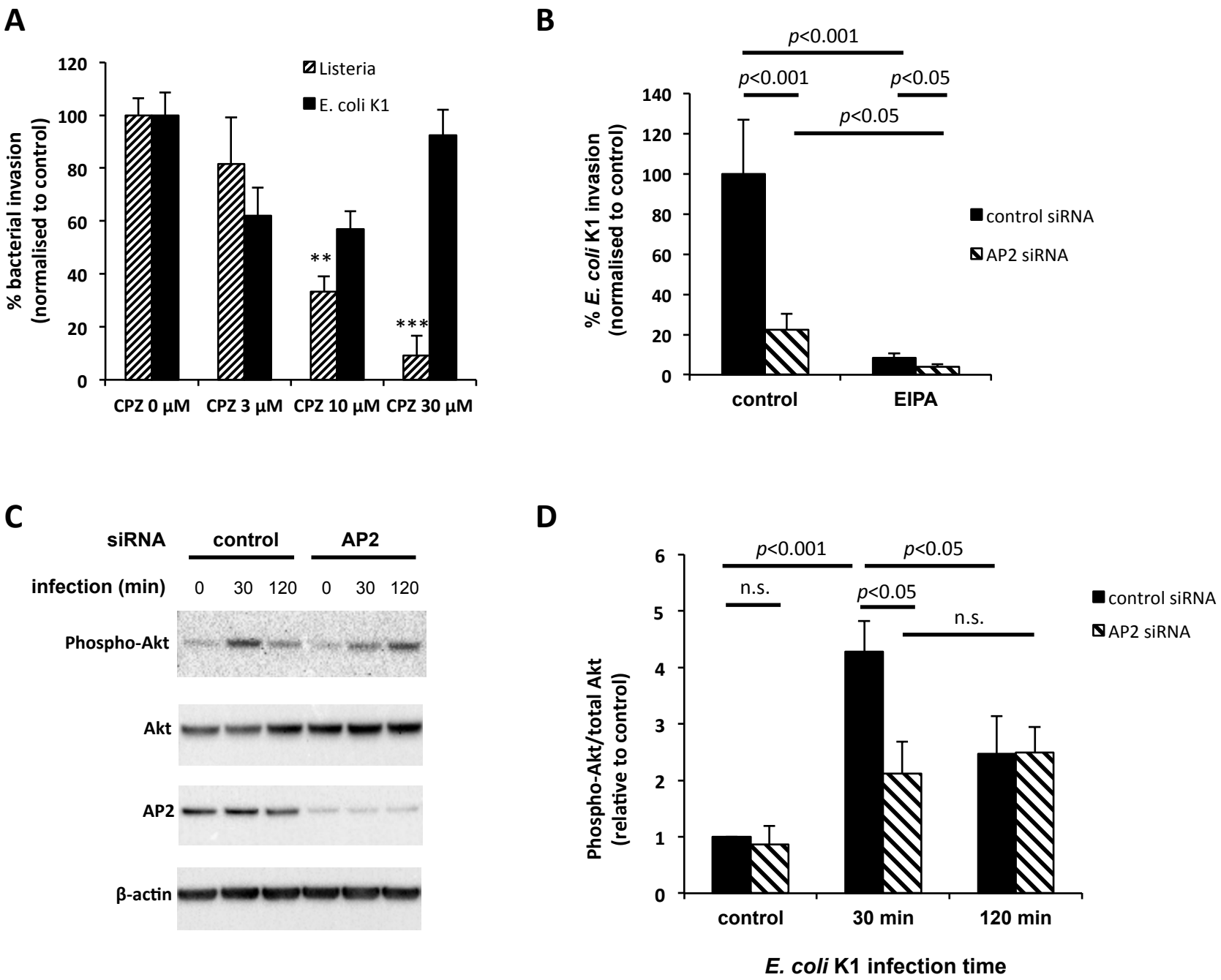

Loh et al Figure 7

Loh et al Figure 8

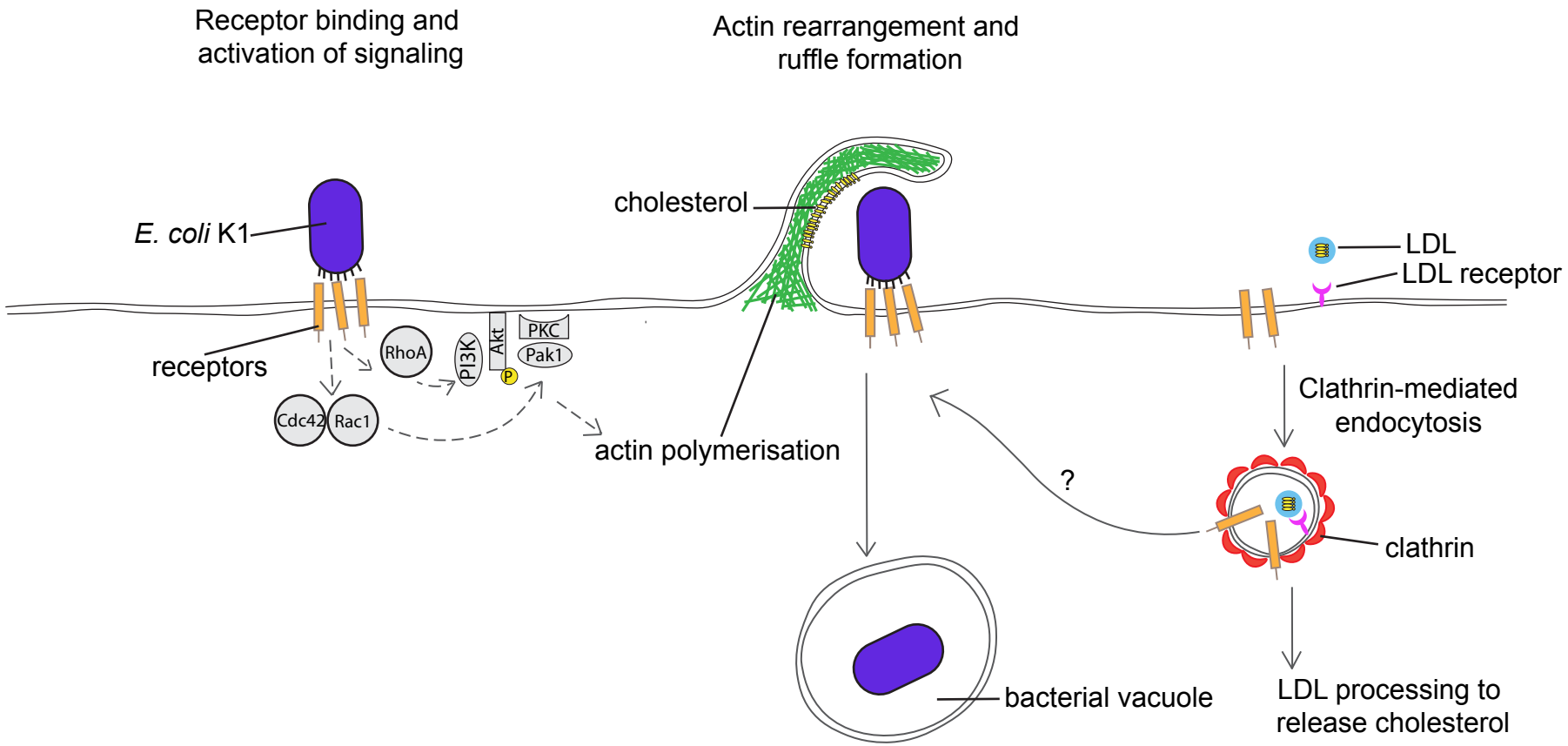

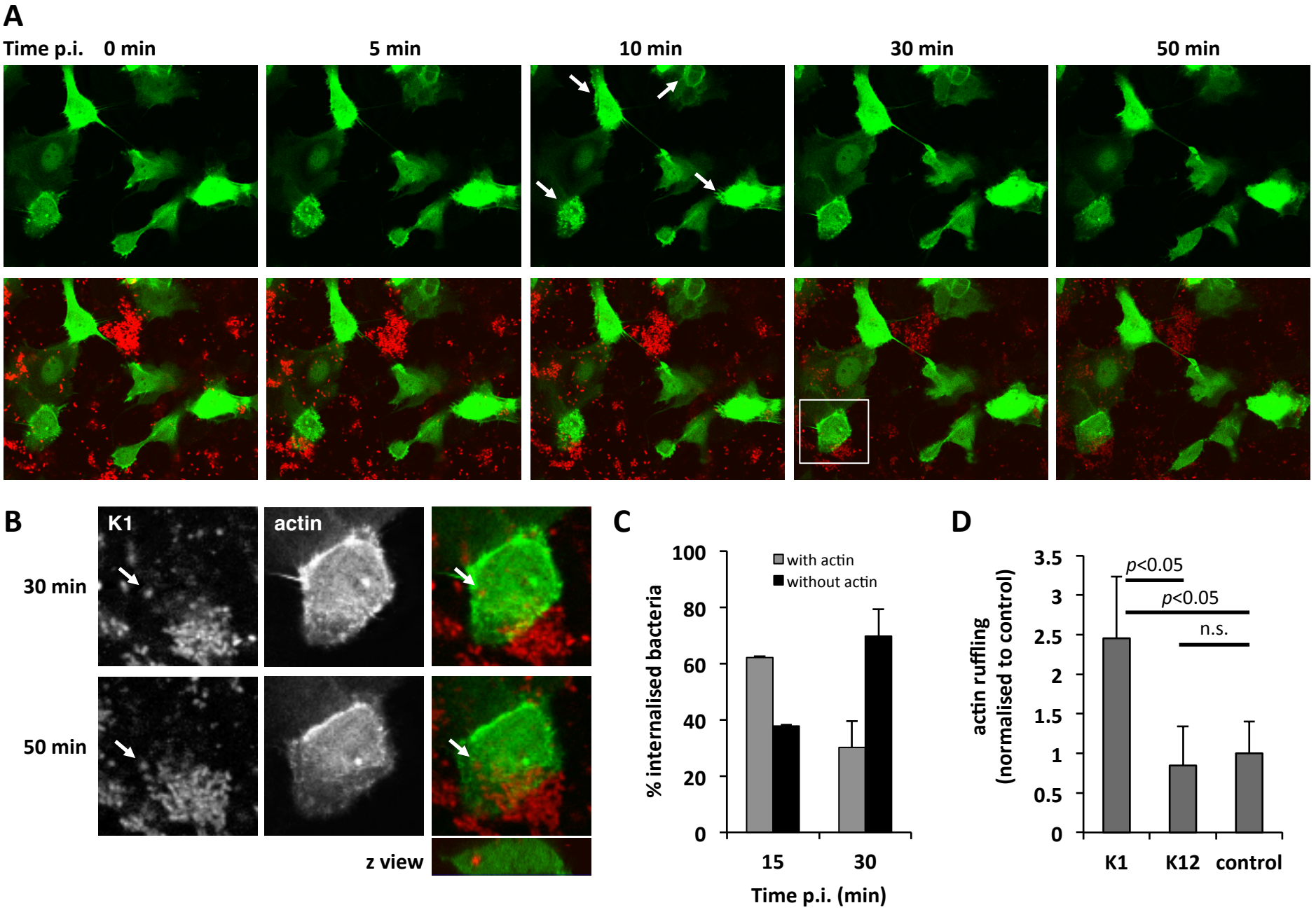

Loh et al Supplementary Figure 1

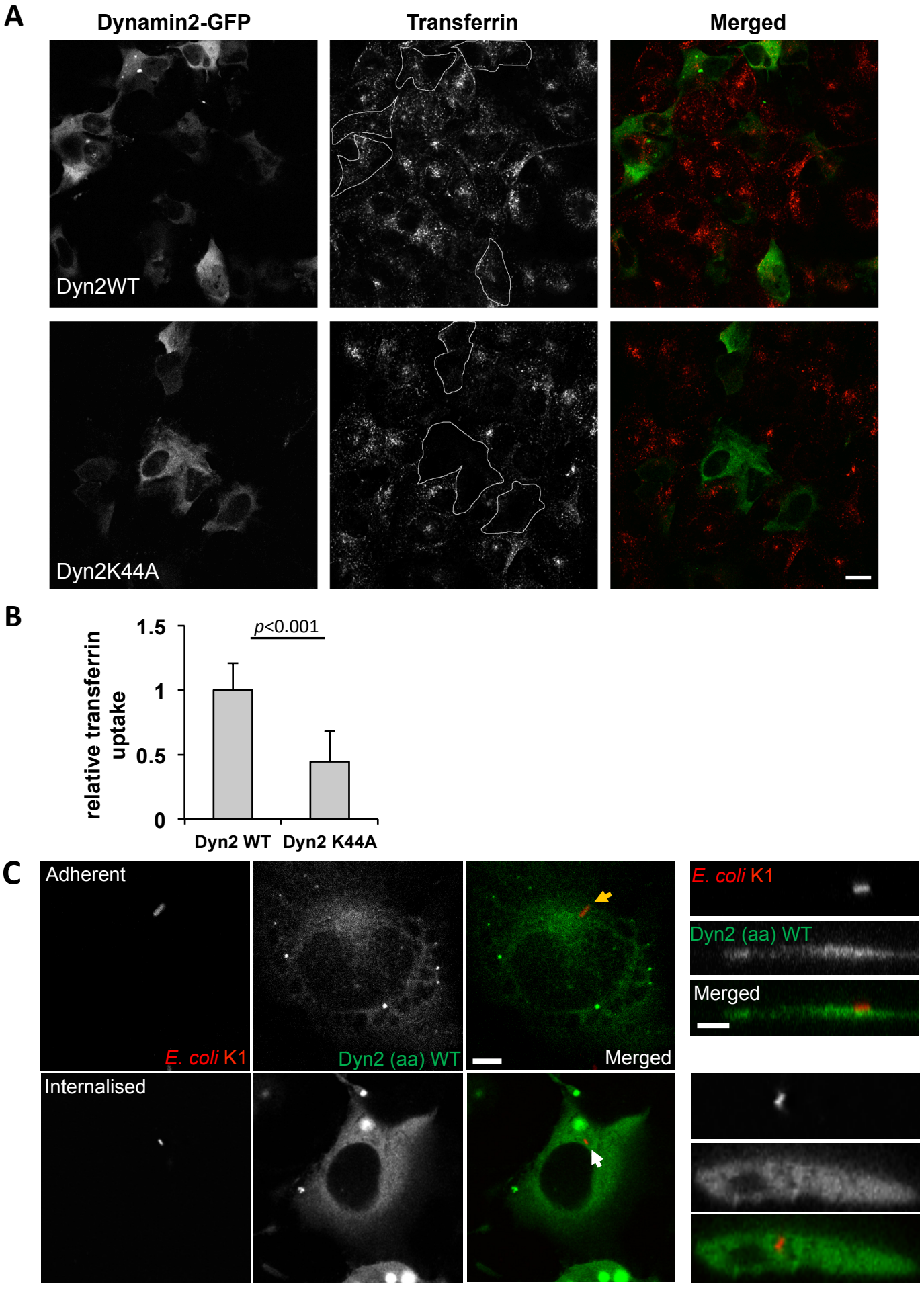

Loh et al Supplementary Figure 2

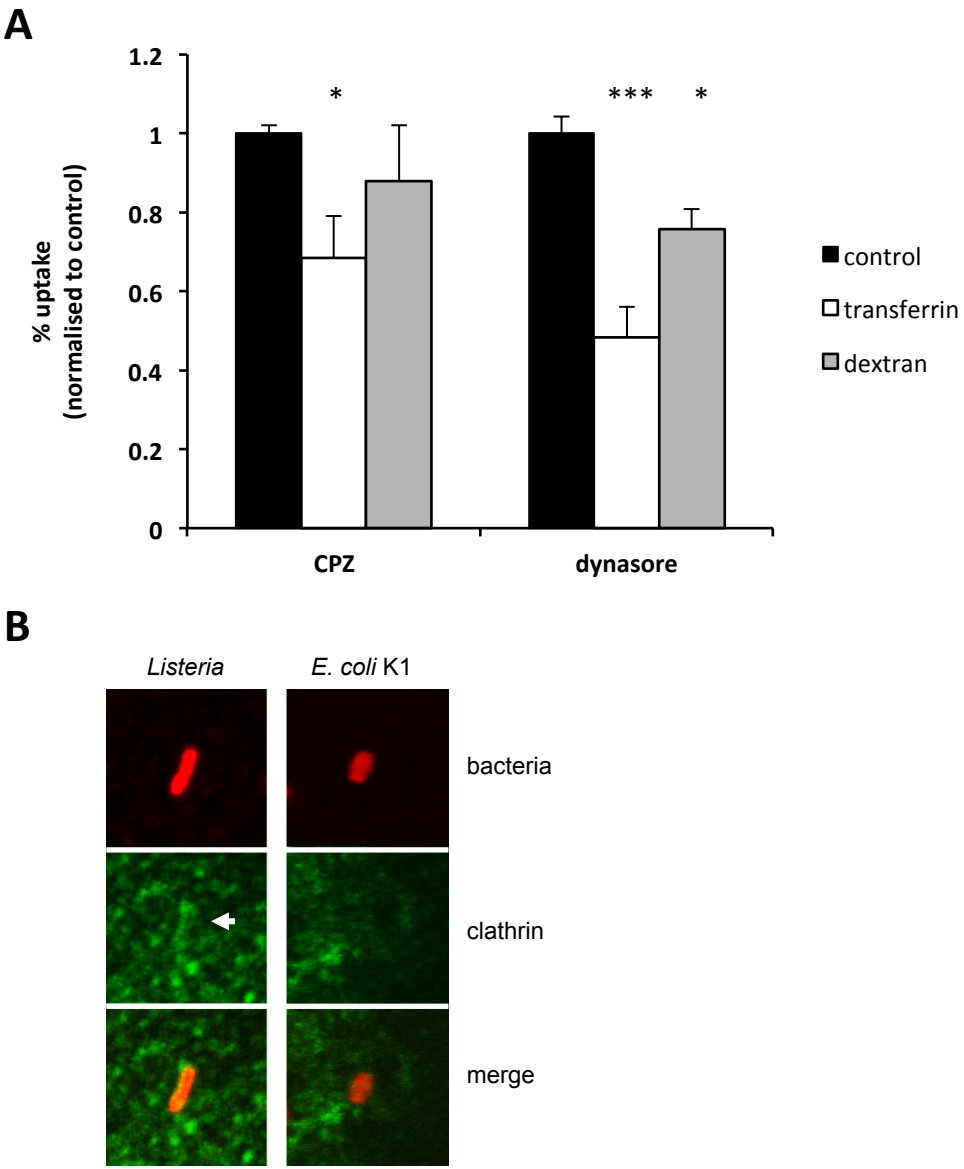

Loh et al Supplemental Figure 3